



EUROPEAN
COMMISSION

Community research

PAMINA

Performance Assessment Methodologies in Application to Guide the Development of the Safety Case

(Contract Number: **FP6-036404**)



FINAL REPORT ON UNCERTAINTY ANALYSIS CODES (D-N°:4.3.1)

Author(s): **ANDRA: D. Perraud, G. Pepin, E. Treille, L. Loth**
JRC: R. Bolado-Lavín, K-F Nilsson, S. Prváková, A. Costescu-Badea

Date of issue of this report: **15/11/09**

Start date of project : **01/10/2006**

Duration : **36 Months**

Project co-funded by the European Commission under the Euratom Research and Training Programme on Nuclear Energy within the Sixth Framework Programme (2002-2006)		
Dissemination Level		
PU	Public	X
RE	Restricted to a group specified by the partners of the [PAMINA] project	
CO	Confidential, only for partners of the [PAMINA] project	



Foreword

The work presented in this report was developed within the Integrated Project PAMINA: **P**erformance **A**ssessment **M**ethodologies **I**N Application to Guide the Development of the Safety Case. This project is part of the Sixth Framework Programme of the European Commission. It brings together 25 organisations from ten European countries and one EC Joint Research Centre in order to improve and harmonise methodologies and tools for demonstrating the safety of deep geological disposal of long-lived radioactive waste for different waste types, repository designs and geological environments. The results will be of interest to national waste management organisations, regulators and lay stakeholders.

The work is organised in four Research and Technology Development Components (RTDCs) and one additional component dealing with knowledge management and dissemination of knowledge:

In RTDC 1 the aim is to evaluate the state of the art of methodologies and approaches needed for assessing the safety of deep geological disposal, on the basis of comprehensive review of international practice. This work includes the identification of any deficiencies in methods and tools.

In RTDC 2 the aim is to establish a framework and methodology for the treatment of uncertainty during PA and safety case development. Guidance on, and examples of, good practice will be provided on the communication and treatment of different types of uncertainty, spatial variability, the development of probabilistic safety assessment tools, and techniques for sensitivity and uncertainty analysis.

In RTDC 3 the aim is to develop methodologies and tools for integrated PA for various geological disposal concepts. This work includes the development of PA scenarios, of the PA approach to gas migration processes, of the PA approach to radionuclide source term modelling, and of safety and performance indicators.

In RTDC 4 the aim is to conduct several benchmark exercises on specific processes, in which quantitative comparisons are made between approaches that rely on simplifying assumptions and models, and those that rely on complex models that take into account a more complete process conceptualization in space and time.

The work presented in this report was performed in the scope of RTDC 4.



Table of contents

1	INTRODUCTION	6
2	DESCRIPTION OF THE BENCHMARKS	7
2.1	CONCEPTUAL MODEL	7
2.1.1	<i>Initial geometry</i>	7
2.1.2	<i>Simplifications and main physical assumptions</i>	7
2.1.2.1	Benchmark 1.....	7
2.1.2.2	Benchmark 2.....	9
2.2	OUTPUT VARIABLE	13
2.2.1	<i>Performance indicators to compute</i>	13
2.2.1.1	Benchmark 1.....	13
2.2.1.2	Benchmark 2.....	15
2.3	ANALYSIS METHODOLOGY.....	16
2.3.1	<i>Input parameters</i>	17
2.3.2	<i>Sampling methods</i>	18
3	METHODOLOGY USED BY EACH PARTICIPANT	19
3.1	ANDRA	19
3.2	JRC-IE	21
4	UNCERTAINTY AND SENSITIVITY ANALYSIS TOOLS AND TECHNIQUES	25
4.1	UNCERTAINTY ANALYSIS	25
4.1.1	<i>Uncertainty analysis tools used</i>	25
4.1.1.1	Numeric statistics	25
4.1.1.2	Graphic tools (time and non time-dependent).....	25
4.1.2	<i>Lessons learnt about UA tools and recommendations</i>	26
4.2	SENSITIVITY ANALYSIS.....	28
4.2.1	<i>Sensitivity analysis tools used</i>	28
4.2.1.1	Regression based statistics.....	28
4.2.1.2	Monte-Carlo filtering techniques (Mann-Whitney & Smirnov tests)	29
4.2.1.3	Graphic tools (scatter-plots, cobweb plots and CSM plots)	29
4.2.2	<i>Lessons learnt about SA tools and recommendations</i>	30
4.2.2.1	Lessons learnt about regression techniques	30
4.2.2.2	Lessons learnt about scatter-plots, cobweb plots and CSM plots.....	32
4.2.2.3	Lessons learnt from the simultaneous use of different SA techniques	33
4.2.2.4	Lessons learnt about the simultaneous use of UA and SA to improve system understanding	34
5	SIMULATION RESULTS AND COMPARISON	36
5.1	RESULTS FROM BENCHMARK 1 – COMPARISON 1D/2D.....	36
5.2	RESULTS FROM BENCHMARK 2 – COMPARISON 2D/3D.....	38
6	COMPLEMENTARY/ALTERNATIVE TECHNIQUE : META-MODELS BASED ON RESPONSE SURFACES	46
6.1	MAIN OBJECTIVE	46
6.2	DESCRIPTION OF THE METHOD (DIFFERENT STEPS)	46
6.3	VALIDATION STEP: COMPARISON WITH MONTE-CARLO/LHS SIMULATIONS	48
6.4	EXAMPLE OF APPLICATION (NEURAL NETWORKS): EFFECT OF SAMPLE SIZE ON THE CONVERGENCE AND ACCURACY OF ESTIMATES	50
7	GENERAL CONCLUSIONS	52
8	REFERENCES	55

List of Figures

Figure 2.1-1 : Initial geometry (ILW and its environment)	7
Figure 2.1-2 : Geometrical assumptions and components/materials (benchmark 1).....	8
Figure 2.1-3 : Geometrical assumptions and components/materials (benchmark 2).....	10
Figure 2.1-4 : States of degradation of concrete material (around waste domain) applied to geochemistry.....	11
Figure 2.1-5 : Way of considering geochemistry {Kd, Csat} in ranges of times for concrete material (around waste domain).....	12
Figure 2.2-1 : Indicators to compute (benchmark 1)	13
Figure 2.2-2 : Indicators to compute (benchmark 2)	15
Figure 2.3-1 : Different steps to perform Monte-Carlo simulations.....	16
Figure 2.3-2 : LHS sampling method (principles with two parameters).....	18
Figure 3.1-1 : Alliances tool used for Monte-Carlo simulations.....	19
Figure 3.1-2 : Grid used for calculations (example of Alliances).....	21
Figure 3.2-1 : Cylindrical geometry of the concept.....	22
Figure 3.2-2 : Vertical slice of the cylindrical geometry	22
Figure 4.1-1 : Ccdfs for the ¹²⁹ I peak molar rate coming out of the argillites (15 m clay) for Alliances and GoldSim	26
Figure 4.1-2 : Evolution over time of 1,000 runs for the ⁷⁹ Se molar rate getting out of the EDZ (Alliances).....	27
Figure 4.1-3 : Evolution over time of key quantiles for the ⁷⁹ Se molar rate getting out of the EDZ (Alliances).....	27
Figure 4.2-1 : SRCs and R ² for the ¹²⁹ I molar rate getting out of the micro-fissured zone (Benchmark 1, GoldSim).....	31
Figure 4.2-2 : SRRCs and R ² for the ¹²⁹ I molar rate getting out of the micro-fissured zone (Benchmark 1, GoldSim)	31
Figure 4.2-3 : Cobweb plot for the ¹²⁹ I peak molar rate at the second radial surface (Benchmark 2, GoldSim).....	34
Figure 4.2-4 : CSM plot for the ¹²⁹ I peak molar rate at the second radial surface (Benchmark 2, GoldSim).....	34
Figure 4.2-5 : 1,000 runs for the ¹²⁹ I molar rate getting out of the micro-fissured zone (Benchmark 2, GoldSim).....	35
Figure 4.2-6 : Rank based regression results for the ¹²⁹ I molar rate getting out of the micro-fissured zone (Benchmark 2, GoldSim).....	35
Figure 5.1-1 : Evolution over time of ¹²⁹ I molar rate getting out of the waste packages (key quantiles, Benchmark 1, Alliances).....	36
Figure 5.1-2 : Evolution over time of ¹²⁹ I molar rate getting out of the waste packages (key quantiles, Benchmark 1, GoldSim)	36
Figure 5.1-3 : Evolution over time of ¹²⁹ I molar rate getting out of the undisturbed argillites, 15 m from the centre of the disposal cell (key quantiles, Benchmark 1, Alliances)	37
Figure 5.1-4 : Evolution over time of ¹²⁹ I molar rate getting out of the undisturbed argillites, 15 m from the centre of the disposal cell (key quantiles, Benchmark 1, GoldSim).....	37
Figure 5.2-1 : Alliances/GoldSim comparison of quantiles of molar rates getting out of 15 m within clay in the case of ¹²⁹ I: a) Alliances and b) GoldSim.....	39
Figure 5.2-2 : Alliances/GoldSim comparison of quantiles of molar rates getting out of the clay layer (top and bottom) in the case of ¹²⁹ I: a) Alliances and b) GoldSim.....	39
Figure 5.2-3 : Alliances/GoldSim comparison of ccdf in the case of ¹²⁹ I: a) out of 15 m clay and b) out of clay layer	40
Figure 5.2-4 : Alliances/GoldSim comparison of quantiles of molar rates getting out of disposal cell along cell/EDZ in the case of ¹²⁹ I: a) Alliances and b) GoldSim.....	40
Figure 5.2-5 : Alliances/GoldSim comparison of quantiles of molar rates getting out of gallery/EDZ in the case of ¹²⁹ I: a) Alliances and b) GoldSim	41
Figure 5.2-6 : Alliances/GoldSim comparison of ccdf in the case of ¹²⁹ I: a) out of disposal cell along cell/EDZ and b) out of gallery/EDZ	41

Figure 5.2-7 : Alliances/GoldSim comparison of ccdf for ⁷⁹Se: a) out of disposal cell in the host rock pathway ; b) out of the clay in the host rock pathway and c) out of gallery/EDZ in the longitudinal pathway..... 43

Figure 6.2-1 : Different steps of creation of meta-models..... 47

Figure 6.3-1 : Validation of meta-models (neural networks, Chaos polynomials) for the maximum ¹²⁹I molar rate coming out of clay 49

Figure 6.4-1 : Application of meta-models (neural networks): sensitivity to the sample size for the Spearman coefficient (for sorption and diffusion in clay)..... 50

List of Tables

Table 2.1-1 : Input data/materials with pdf taken into account for the probabilistic calculations..... 13

Table 3.2-1 : Correlated input parameters considered in the JRC calculations..... 24

Table 4.1-1 : Quantiles for the ¹²⁹I peak molar rate coming out of the argillites (15 m clay) for GoldSim 26

Table 4.2-1 : Most important SA results obtained by JRC in benchmark 2 for the ¹²⁹I peak molar rate at the second radial surface via regression analysis and MCF 33

Table 5.2-1 : The three most important rank indicators and their values for the ¹²⁹I peak molar rate at three interfaces..... 43

Table 5.2-2 : The three most important rank indicators and their values for the ⁷⁹Se peak molar rate at three interfaces..... 44

1 Introduction

JRC-IE and Andra collaborate in the Framework of the Integrated Project PAMINA (Performance Assessment Methodologies in Application to Guide the Development of the Safety Case) to develop and apply advanced methods for performance assessment of a clay repository [1]. The idea is to apply state-of-the-art techniques of different levels of complexity to assess the performance of a French clay repository and to assess the applicability of different methods. This is done by computing i) how uncertainties in input data affect output (the molar rate of radionuclides in specific parts of the repository system) and ii) to perform sensitivity analysis to rank the processes and input parameters with respect to their relevance for the output.

Data used as input to the analyses are based on the large French research programme for a repository in a Cavollo-Oxfordian clay formation, which is the potential host-rock in France [2]. The JRC and Andra perform analysis in parallel applying their own methods on two benchmarks that have been jointly defined. The benchmarks define the geometry of the system and its constituents, the processes to be considered, the probabilistic density functions of the data, the coupling between parameters and the output to be computed. A first benchmark on a 2D simplified geometry has been performed and also used to calibrate the models, the computational tools and set up the computational methods (report provided by mid-February 2008 as milestone M4.3.2). A second benchmark on a more realistic 3D geometrical description has then been performed (report provided at the end of September 2009 as milestone M4.3.5). A simplified description of the relevant processes is given in [6] and [7]. For the uncertainty analysis the main indicators that are computed include quantiles of the molar rate for a limited number of radionuclides in different parts of the system and complete probability density functions at specific times. The main indicators for the sensitivity analysis include scatter plots for selected parameters, ranking of parameters with respect to their influence on the output and computation of statistical coefficients such as (i) Pearson correlation coefficient, standardised regression coefficient (SRC) and partial correlation coefficient (PCC) to relate input uncertainty to output uncertainty and (ii) Spearman coefficient, standardised rank regression coefficient (SRRC), partial rank correlation coefficient (PRCC) to measure the monotony between uncertainty on the input parameters and uncertainty on the output result, and Monte-Carlo filtering statistics (Mann-Whitney and Smirnov tests), cobweb and CSM plots. In addition, complementary or alternative techniques such as meta-models based on the response surfaces have also been explored (neural networks, Chaos polynomials).

2 Description of the benchmarks

2.1 Conceptual model

2.1.1 Initial geometry

The benchmarks are based on the study of the release of radionuclides from wastes of an ILW disposal cell embedded in a porous material for a generic French clay site. The disposal cell, which only contains non-organic waste forms, does not release any hydrogen gas; it includes both activated waste and compacted hulls and end-caps that are supposed to be homogeneously filled. Figure 2.1-1 represents the typical ILW disposal cell and its environment.

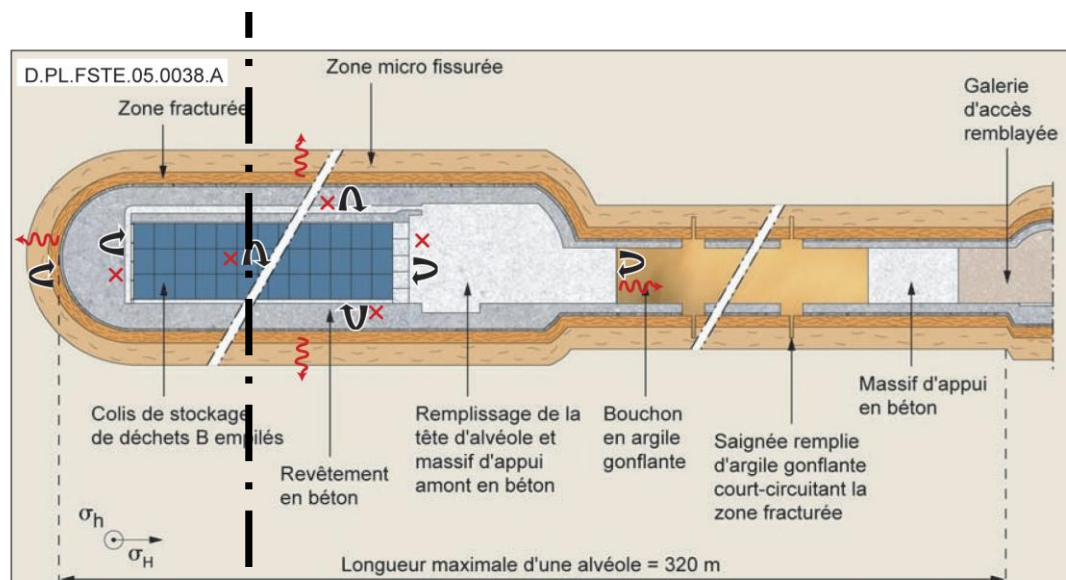


Figure 2.1-1 : Initial geometry (ILW and its environment)

2.1.2 Simplifications and main physical assumptions

2.1.2.1 Benchmark 1

For the first benchmark exercise, a simplified representation of the disposal cell has been considered (see Figure 2.1-2). It consists of a 2D vertical slice of the “middle” of the disposal cell dealing with the host rock pathway only. The complete geometrical model includes the thickness (130 meters) of the undisturbed host rock (Callovo-Oxfordian layer) and the disposal cell located in the middle of the clay layer. The waste packages domain is considered as a rectangle located in the centre of the circular disposal cell. The materials considered in the benchmark model are also indicated in Figure 2.1-2.

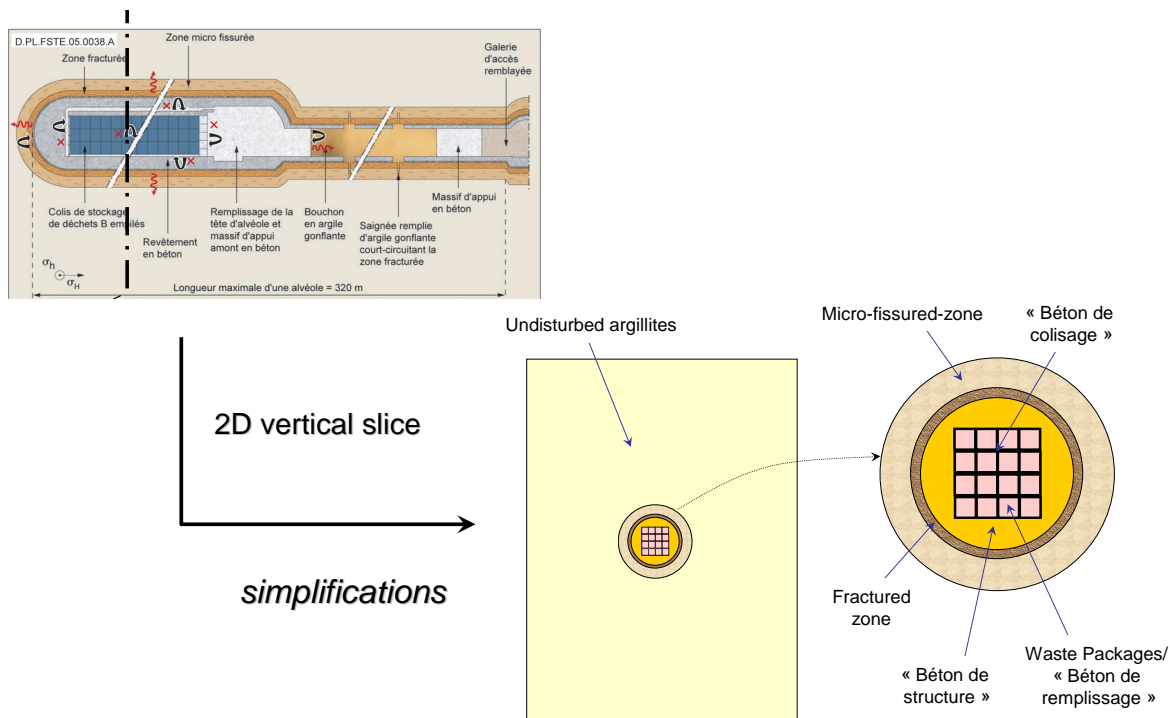


Figure 2.1-2 : Geometrical assumptions and components/materials (benchmark 1)

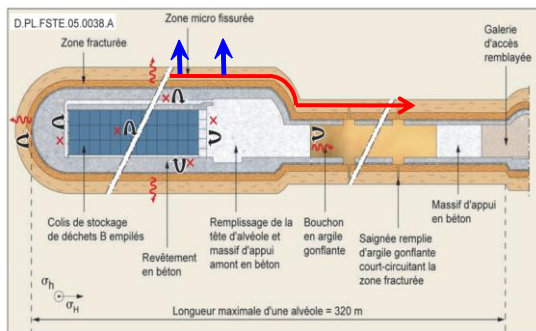
The main assumptions taken into account in the calculations are:

- Materials within the disposal cell and its environment are considered as homogeneous and continuous porous media, and are supposed to be water saturated from $t=0$; hence release of radionuclides from waste packages starts from $t=0$. Calculations are carried out up to 1 million years.
- The migration of radionuclides in porous media in the aqueous solutions is considered as convective/diffusive/dispersive, taking into account phenomena of sorption (linear and reversible, K_d approach) and chemical precipitation (solubility limit C_{sat}). The convective part is based on steady-state hydraulic results using constant ascending vertical head gradient through the host rock.
- The waste package is represented by two materials: (i) a specific concrete filling (“béton de remplissage”), in which the source term is distributed in an uniform way, and for the migration there is no sorption and solubility is unlimited from $t=0$ and; (ii) an over-pack in a specific concrete (“béton de colisage”) with a high level of confining performances (low diffusivity, high K_d and low solubility limit) up to 10.000 years, and then degrading itself into filling concrete (“béton de structure”). Thus the material properties in the analysis will change at this time. The details for this are given in [6].

- The ILW disposal cell around the waste domain is filled with a concrete material in which radionuclides are free to migrate with no hydraulic/transfer performance (high permeability and diffusivity) except for geochemistry. Thus, no uncertainty has been considered, like “béton de remplissage” (with same deterministic input data), except for geochemistry (see next paragraph).
- A relevant approach of the geochemical characterization would be a variation in space and time of K_d and C_{sat} taking into account the evolution of different states of concrete (sound, altered, degraded, neutralised conditions). Since the dynamics of propagation of the various alterations of concrete are not known, we consider, for the first benchmark, only one geochemistry which is applied to all the thickness of concrete (all the disposal cell) and whose spectrum of variation (uncertainty) takes into account the various alterations. This is applied by ranges of time.
- The mechanical disturbance is represented by the Excavated Damaged Zone (EDZ), which consists of a fractured zone with high permeability and of a micro-fissured zone, whose extensions are perennial in time. The occurrence of a self-sealing phenomenon is integrated into the uncertainty (probabilistic density function).
- The chemical disturbance generated by the degradation of the concrete is included in the mechanical disturbance (EDZ), in terms of extension and in hydraulic/transfer parameters. The geochemistry considered in the EDZ is the same as in the undisturbed argillites.

2.1.2.2 *Benchmark 2*

For the second benchmark exercise, a more realistic representation of the disposal cell is considered (see Figure 2.1-3). It consists of a 3D model including both pathways: the first one (in blue color) through the host rock (as in Benchmark 1) and the second one (in red color) along the disposal cell towards the gallery. The complete geometrical model includes the thickness (130 meters) of the undisturbed host rock (Callovo-Oxfordian layer) and the disposal cell located in the middle of the clay layer. The waste packages domain is considered as a parallelepiped located in the centre of the disposal cell. The materials to be considered in the benchmark model are also indicated in Figure 2.1-3.



Host rock pathway (radial)

Along disposal cell pathway (axial)

Simplified 3D model including both pathways

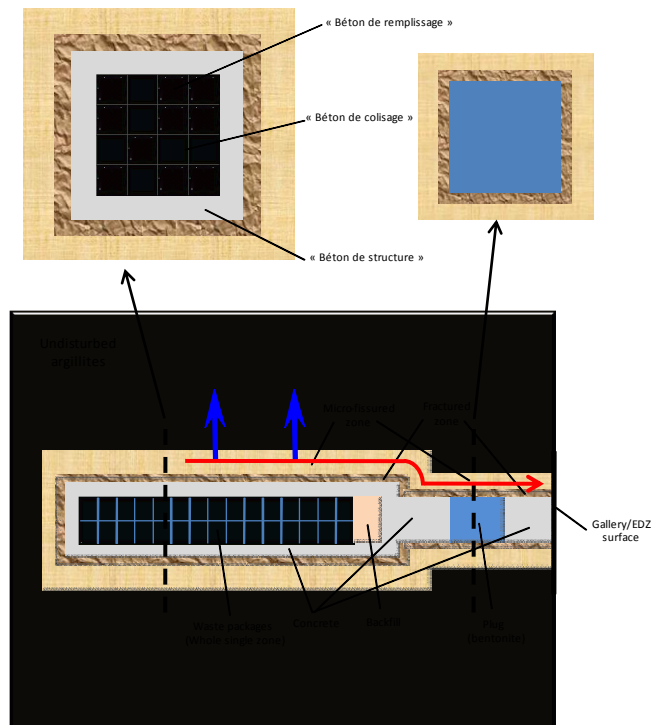


Figure 2.1-3 : Geometrical assumptions and components/materials (benchmark 2)

The main assumptions taken into account in calculations are the same as for Benchmark 1 except for the following points (the details for this are given in [7]):

- The waste package is represented by one material with no distinction between concrete filling (“béton de remplissage”), in which the source term is distributed in a uniform way, and over-pack (disposal container) concrete (“béton de colissage”). For migration in this material, there is no hydraulic/transfer performance (high permeability and diffusivity corresponding to a neutralized concrete: $K = 10^{-6}$ m/s and $D_p = 2.10^{-9}$ m²/s). Only geochemistry is applied in the domain, using {Kd, Csat} approach on the basis of deterministic input data. It is the same for backfill properties.
- For concrete material in the disposal cell around the waste domain, a specific geochemistry is considered, with a distribution coefficient (Kd) and a solubility limit (Csat). The various studies of geochemical characterization of the concretes show that the retention varies according to the various states of alteration of the concrete (sound, altered, degraded, neutralized conditions). A relevant approach would be thus a variation {space/time} of {Kd, Csat} taking into account these various

conditions as shown on Figure 2.1-4. Dynamics of propagation of the various alterations of concrete have been performed with many types of concrete. For this second benchmark, according to physical studies applied to concrete chemical degradation, three chemical states are considered (sound, altered, degraded) and the neutralized one can be overlooked. The upper part of Figure 2.1-5 gives typical evolution of geochemical states {space/time} and the lower part shows the slightly simplified assumptions used in the analysis. This has been applied only to ^{79}Se and leads to a more detailed discretization of the disposal cell zone around the waste domain, that is to say a new mesh. For ^{129}I , the solubility limit is infinite and K_d is supposed to be independent from the states of degradation of the concrete material.

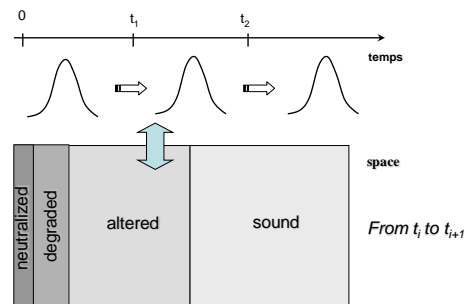


Figure 2.1-4 : States of degradation of concrete material (around waste domain) applied to geochemistry

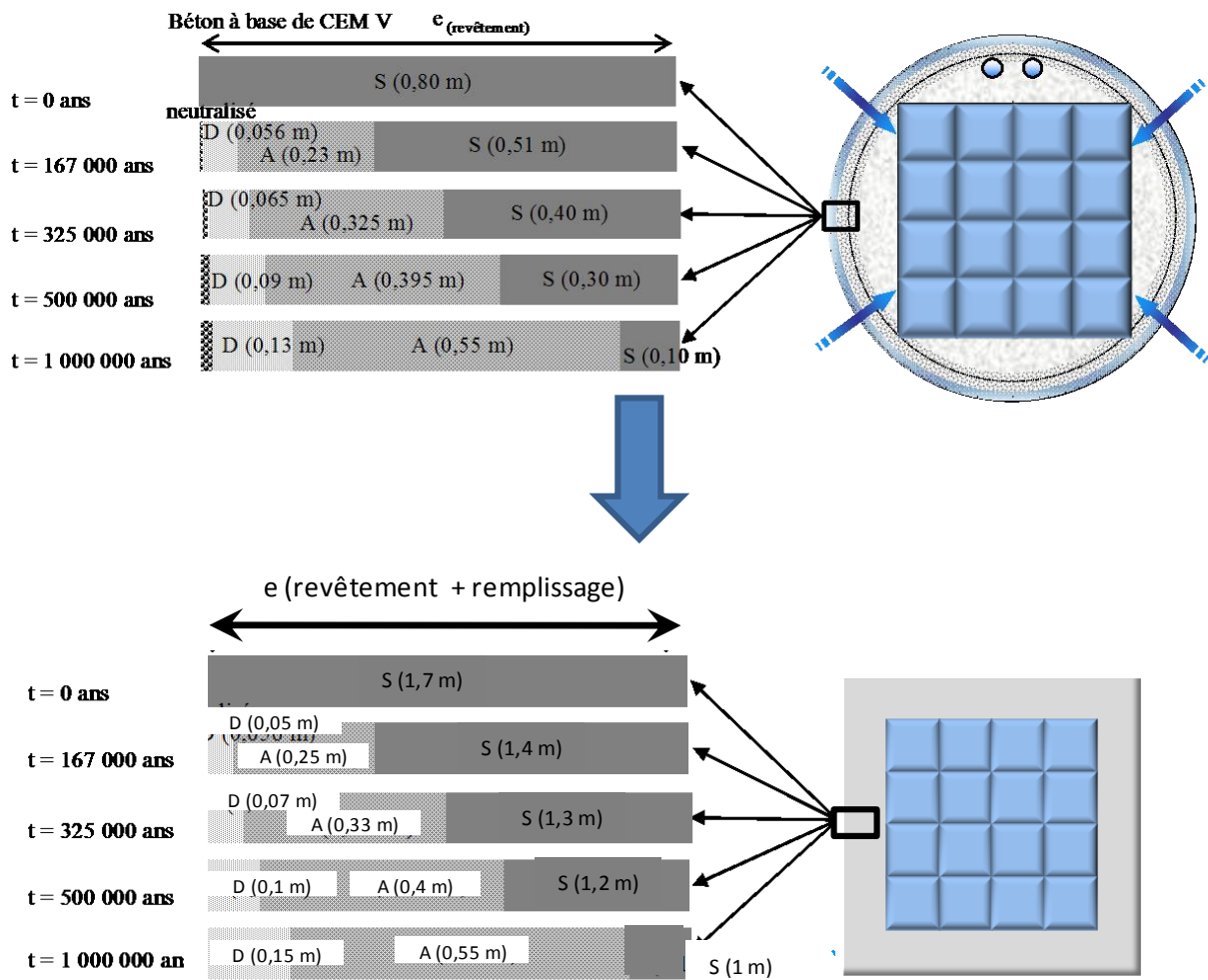


Figure 2.1-5 : Way of considering geochemistry $\{K_d, C_{sat}\}$ in ranges of times for concrete material (around waste domain)

Taking into account the previous topics, Table 2.1-1 gives probabilistic input data that have been considered within the second benchmark calculations (as an example):

	Undisturbed argillites	Micro-fissured zone	Fractured zone	Concrete	Bentonite
<i>Release rate of metallic components</i>	× (corrosion rate)				
<i>Permeability</i>	× (horizontal/ vertical)	×	×		×
<i>Effective diffusion coefficient</i>	×	×	×		×
<i>Head ascending vertical gradient in undisturbed argillites</i>	×				
<i>Distribution coefficient</i>		×		× {space/time} dependent for ⁷⁹ Se and ⁹⁴ Nb × constant for ¹²⁹ I (concrete in disposal cell around the waste domain)	×
<i>Solubility limit</i>		×		× {space/time} dependent for ⁷⁹ Se and ⁹⁴ Nb (concrete in disposal cell around the waste domain)	× (idem argillites)
<i>Diffusion porosity</i>	×	×	×		×

Table 2.1-1 : Input data/materials with pdf taken into account for the probabilistic calculations

2.2 Output variable

2.2.1 Performance indicators to compute

2.2.1.1 Benchmark 1

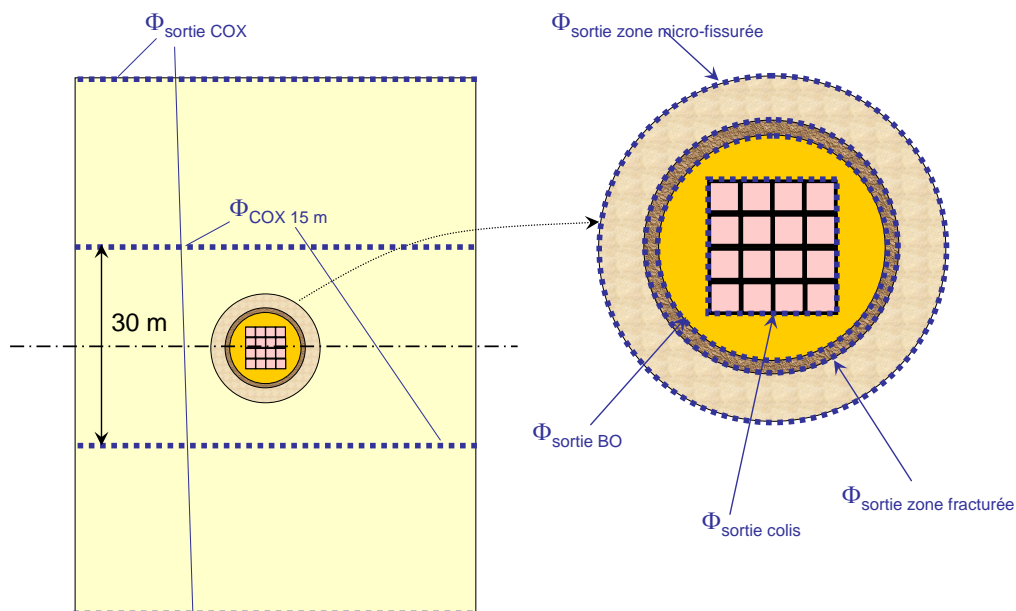


Figure 2.2-1 : Indicators to compute (benchmark 1)

The different types of physical indicators computed for the first benchmark are the molar rates (Figure 2.2-1) coming:

- out of the waste packages $\Phi_{\text{sortie colis}}$ (external envelope surface of waste packages pile),
- out of the disposal cell $\Phi_{\text{sortie BO}}$ (external envelope surface of « béton de structure » material),
- out of the fractured zone $\Phi_{\text{sortie zone fracturée}}$ (external envelope surface of fractured zone material),
- out of the micro-fissured zone $\Phi_{\text{sortie zone micro-fissurée}}$ (external envelope surface of micro-fissured zone material),
- out of the undisturbed argillites, in the clay $\Phi_{\text{COX 15m}}$, at a specific surface located at 15 meters from packages, and from the undisturbed argillites, $\Phi_{\text{sortie COX}}$ (top and bottom).

A statistical analysis has been carried out for the evolution of the molar rates previously defined and a more detailed analysis has been done for:

- the maximal release of radionuclides (molar rate) between 0 and 1.000.000 years,
- the occurrence of the maximal release (molar rate) between 0 and 1.000.000 years.

Statistical indicators for uncertainty analysis of the results are:

- the evolution (in time) of the various (physical) indicators with quantiles at 1%, 5%, 25%, 50% (median), 75%, 95%, 99% plus the mean,
- the probability density function (pdf), the cumulative probability density function (cdf), complementary cumulative distribution function (ccdf) of the various physical indicators; the peak value for each distribution and the time when that maximum occurs ; and with characterization of the various moments of order 3 and 4 (skewness coefficient and kurtosis) of the distributions.

The objective of the sensitivity analysis is to rank the input parameters with respect to their importance to the radionuclide migration and how they affect the output indicators. The analysis is made by means of specific statistical coefficients:

- coefficients measuring the linearity between the uncertainty of the result and the uncertainty of input data : Pearson correlation coefficient, partial correlation coefficient (PCC) and standardised regression coefficient (SRC),

- coefficients measuring the monotony between the uncertainty of the result and the uncertainty of the input data : Spearman correlation coefficient, partial rank correlation coefficient (PRCC) and standardised rank regression coefficient (SRRC).

2.2.1.2 Benchmark 2

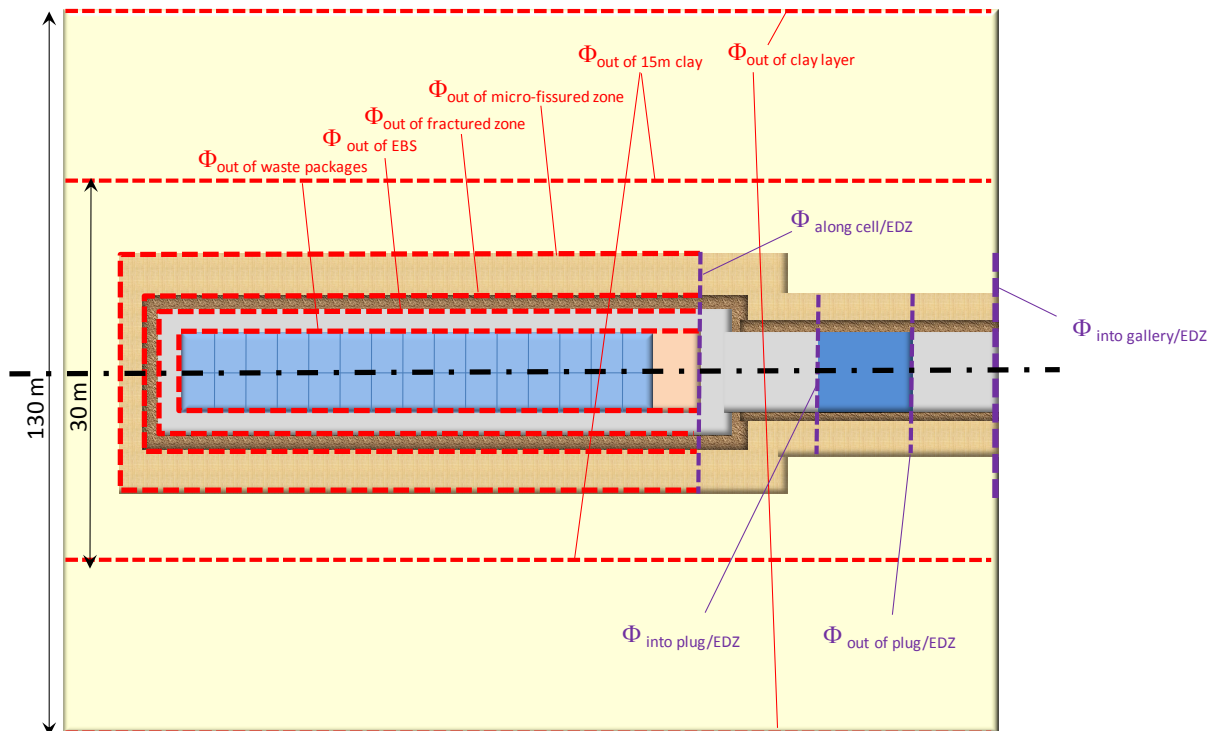


Figure 2.2-2 : Indicators to compute (benchmark 2)

The different types of physical indicators computed for the second benchmark are the molar rates (Figure 2.2-2) coming:

- out of the waste packages $\Phi_{\text{out of waste packages}}$ (external envelope surface of waste packages pile),
- out of the disposal cell $\Phi_{\text{out of EBS}}$ (external envelope surface of disposal cell « béton de structure » material),
- along the disposal cell including EDZ $\Phi_{\text{along cell/EDZ}}$ (surface on the right side of the backfill including EDZ),
- out of the fractured zone $\Phi_{\text{sortie zone fracturée}}$ (external envelope surface of fractured zone material),

- out of the micro-fissured zone $\Phi_{\text{out of micro-fissured zone}}$ (external envelope surface of micro-fissured zone material),
- out of the undisturbed argillites in the clay $\Phi_{\text{COX 15 m}}$ (at a specific surface located at 15 meters from packages),
- out of the undisturbed argillites $\Phi_{\text{out of clay layer}}$ (at the top and bottom),
- into plug and EDZ $\Phi_{\text{into plug/EDZ}}$ (left side of bentonite plug),
- out of plug and EDZ $\Phi_{\text{out of plug/EDZ}}$ (right side of bentonite plug),
- into gallery/EDZ $\Phi_{\text{into gallery/EDZ}}$ (entrance of the gallery including disposal cell EDZ).

2.3 Analysis Methodology

Monte-Carlo methods will be adopted in this benchmark. Their main advantages include: i) it is user-friendly and straightforward to understand and implement; ii) the possibility to consider the spectrum of variation of all parameters to investigate; iii) to carry out both uncertainty and sensitivity analysis and to offer a wide range of graphic output possibilities. The Monte Carlo methodology is based on several steps with pre-processing, processing and post-processing as outlined in Figure 2.3-1.

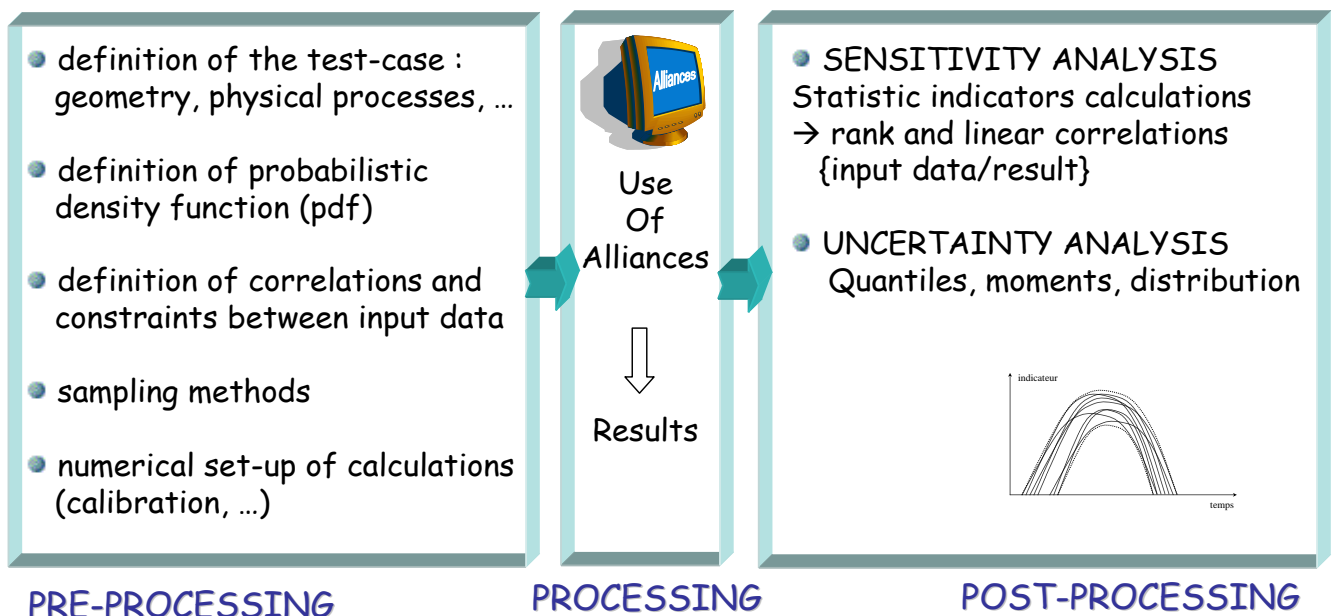


Figure 2.3-1 : Different steps to perform Monte-Carlo simulations

2.3.1 *Input parameters*

After having set up the physical and geometrical characteristics of the benchmark, probabilistic density functions (pdfs) need to be defined for the parameters with uncertainty. The pdfs used in this Benchmark are based on a large data set from an intensive characterization programme in Andra in combination with expert judgment and/or literature review. The pdfs include three sources of uncertainty: natural variability (especially for argillites), experimental measurement methods (laboratory + in situ tests) and up-scaling (extrapolation from small samples to repository scale). All pdfs are truncated. The pdfs are given in [6] and [7].

The models used for the calculations include many input data that are coupled. In order to obtain the most physical coherence for each set of input data, correlations and constraints are defined to prescribe natural constraints and couplings between data, and that need to be taken into account when defining the samples. Two basic types of correlations can be distinguished (statistical and static) as well as constraints. A short description is given below:

- **statistical correlation:** is a measure of the linear association between two input parameters. It may vary from -1 to +1. The ± 1 refer to perfect linear relation with positive or negative slope. Zero means that there is no statistical correlation.
- **static correlation:** this type of correlation makes it possible to bind two stochastic variables by a function or a scalar. For example, the horizontal permeability of the undisturbed argillites results from the vertical permeability via an "anisotropy" function, itself sampled [6] [7].
- **constraints** between stochastic parameters are identified in order to impose the physical coherence of sets of input data; it consists of applying inequalities between the data, after having used first the statistical correlation. If the constraint is not respected at the end of the sampling (taking into account correlations), then the value of the data is equal to the extreme of the inequality. Consequently some initial pdfs might be affected when using constraints. The constraints are detailed in [6] and [7].

2.3.2 Sampling methods

Two different sampling methods have been used for the benchmarks. Andra has used the Latin Hypercube Sampling (LHS). Each marginal probability density function (pdf) is cut out into equiprobable layers and a SRS of size 1 is taken in each layer. The complete sample is obtained by generating a permutation of each marginal sample and combining all the marginal samples at random. The LHS method (see Figure 2.3-2) enables to cover the total spectrum of variation of the different parameters. JRC has used the Simple Random Sampling (SRS).

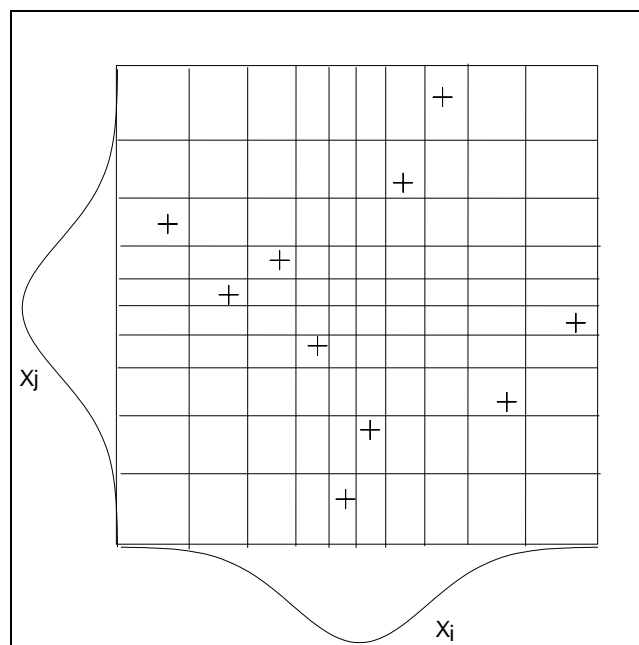


Figure 2.3-2 : LHS sampling method (principles with two parameters)

3 Methodology used by each participant

3.1 Andra

Hydraulic and transport of radionuclides were performed by using the Alliances platform. Alliances platform (Figure 3.1-1) co-developed by Andra, CEA, and EDF since 2001, is used to perform calculations and carry out studies on multi-physic and multi-scale behaviour of a waste repository and its environment. Alliances platform is divided into several “modules”, in which several codes can be used to compare results. For this benchmark, the hydraulic/transport module has been used; Porflow code has been used for hydraulic and solute transport under saturated conditions (in advection/diffusion/dispersion, using radioactive decay, adsorption and solubility limit).

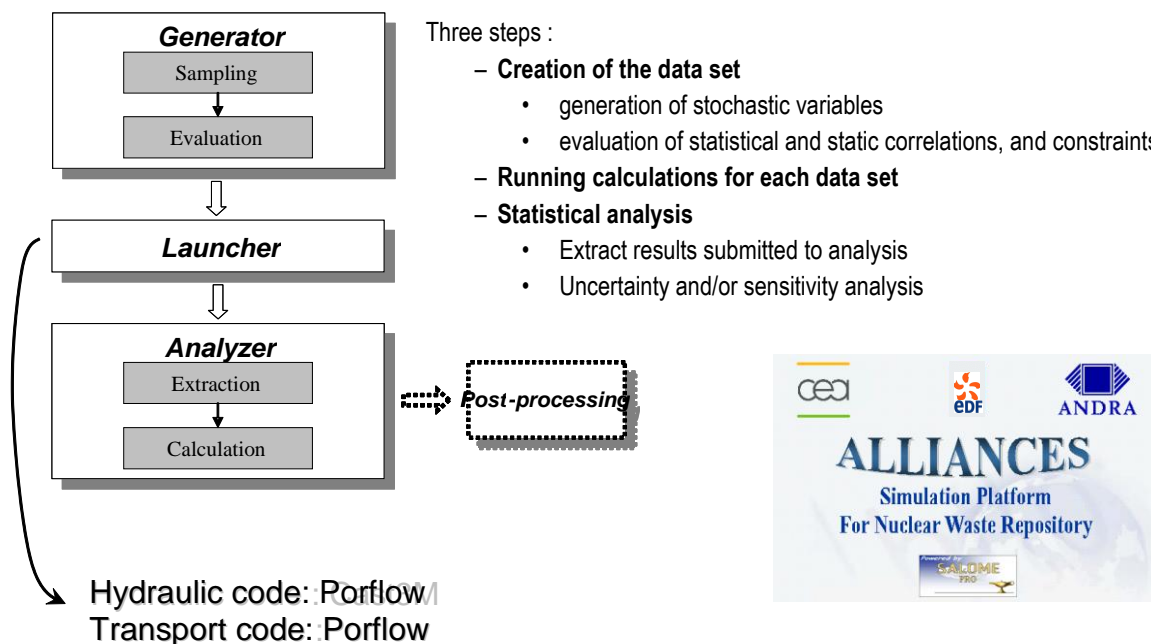


Figure 3.1-1 : Alliances tool used for Monte-Carlo simulations

Calculations have consisted of:

- generating the first sets of input data by LHS method,
- generating the sets of input data to be performed (after having rearranged the first sets using correlations - static, statistic, and inequalities due to constraints),

- running calculations using Porflow,
- extracting results (molar rates in time and maximal molar rate, times of maxima, ...),
- calculating statistical indicators for:
 - uncertainty analysis : quantiles, pdf and ccdf,
 - sensitivity analysis (Pearson, PRC, SRC, Spearman, PRCC, SRRC).

All physical and statistical characteristics have been taken into account in calculations. The details are given in [6] and [7].

Good time steps are calibrated to cover the whole range of variation and especially for short times, to have a good description of the source term. In addition, for the calculation, the number of time steps has been optimized in order to have reasonable calculation times, especially for ^{79}Se for which the mesh is bigger due to the variation of geochemical parameters in concrete.

On the other hand, related to the range of input data, we have to pay attention to ensure a good numerical convergence, finding the best compromise {spatial and time discretization / solver / required accuracy} with physics. Two different grids, rectangular meshes containing around 398 500 and 573 000 elements have been used for the calculations (^{129}I and ^{79}Se respectively), based on the strongest constraints, and based on mesh Peclet Number, skewness, etc. The Figure 3.1-2 shows the grid used for ^{79}Se including a detailed view of the disposal cell and gallery (for visualization, a scale factor of 5 has been applied in the direction perpendicular to the disposal cell axis).

Routines have been developed for post-processing, to check good convergence (mass balance within each material, ...).

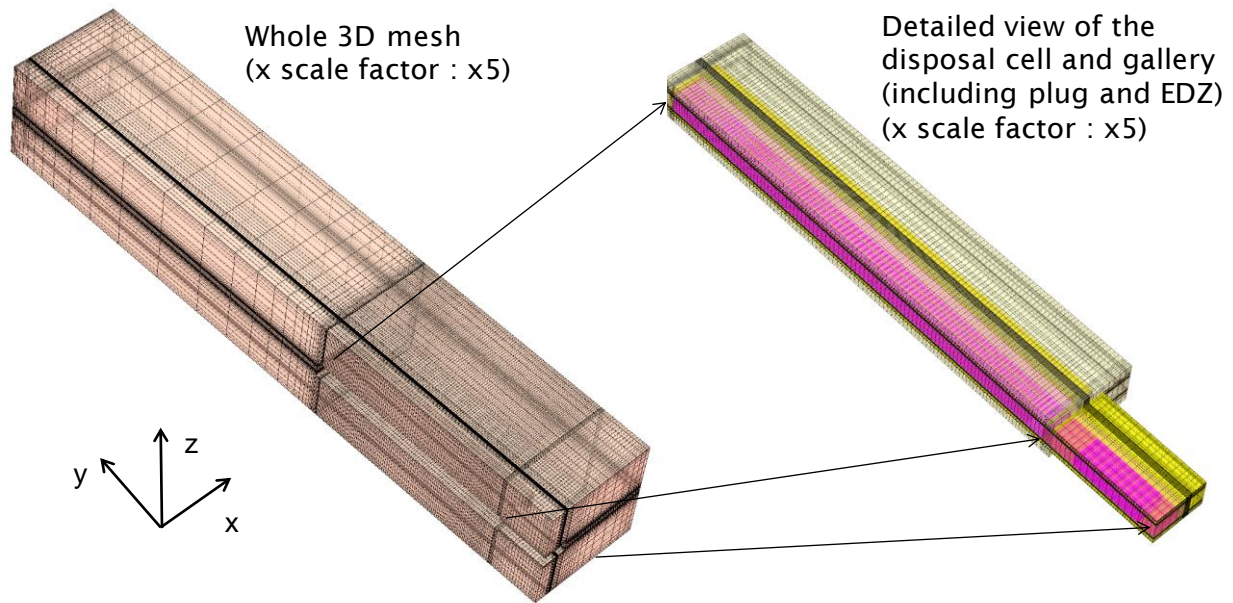


Figure 3.1-2 : Grid used for calculations (example of Alliances)

3.2 JRC-IE

Transport of radionuclides was performed using the commercial code GoldSim, which is a compartment mass transport model tool designed for dynamic and probabilistic simulation of contaminants migration within an environmental system. The user defines basic elements (so called cells) that describe the geometry and material properties of the system and how these elements are connected. Goldsim can describe rather complex systems but there are certain limitations with respect to geometry, processes and couplings between processes and parameters. The geometrical description is restricted to the cylindrical or planar 2-D geometries with possibility to be extruded to the third direction. The repository in this case is modelled by cylindrical cells extended in the axial direction (cf. Figure 3.2-1). The computed properties, in our case the molar rate, therefore have two degrees of freedom: radial and axial. Total number of cells is slightly more than 1000 with approximately 41 and 27 elements in the axial and radial direction respectively. The accuracy of the numerical results increases with the number of elements but the computational cost increases as well. The number of cells we use is therefore a compromise between reasonable accuracy and computational time for the Monte Carlo simulations. Time dependable material properties and large gradients of the molar rate in certain areas require finer discretization of the geometry. The cell elements are therefore smaller within a material with large variation of the material properties in time and space (e.g. concrete degradation) and at the boundaries between

materials but very large within the undisturbed argillites layer. In the axial direction the cell size varied from 0.1 m to 12 m and in the radial direction from 0.03m to 10m.

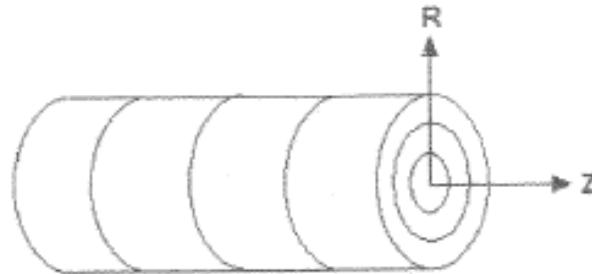


Figure 3.2-1 : Cylindrical geometry of the concept

In the Benchmark 2, the cross section of the different components in the disposal cell is square. In the Goldsim model each cross section is modelled as cylindrical but with the same "diameters" as in the Benchmark 2 definition used by Andra. Consequently the surfaces between components are smaller in the Goldsim model than the Andra's one by a factor $\pi/4$. The adopted cross sections are shown in Figure 3.2-2.

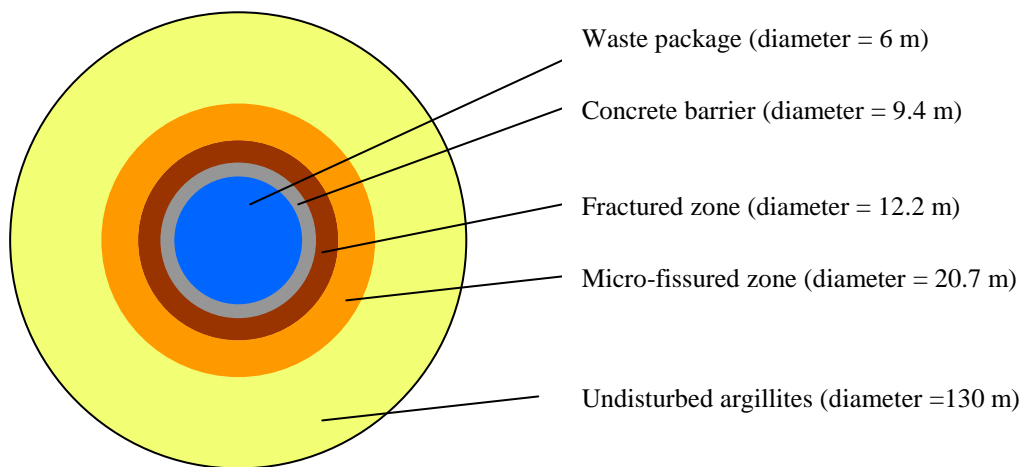


Figure 3.2-2 : Vertical slice of the cylindrical geometry

Diffusion is the dominant radionuclide migration process. This is definitely expected to be the case for the host rock pathway whereas for the disposal cell pathway advection will also play certain role. Goldsim is a mass transport model tool and can therefore not perform any hydrological calculations. Advective flow rates in the form of Darcy velocities were therefore calculated separately using Darcy velocities provided by Andra in the following way. The Darcy velocity Q , depends linearly on the hydraulic conductivity, K , the cross sectional area to the flow, S , and the hydraulic gradient, $grad h$ ($Q = -K \cdot S \cdot \nabla h$). Andra provided the value

of the Darcy velocity and hydraulic conductivity for each material for a particular case. This allowed us to compute the hydraulic gradient for given material, $\nabla h^* = -Q^* / (K^* \cdot S^*)$. This value of the head gradient for each material was kept for all simulations and the Darcy velocity in each cell was computed from the Darcy equation using the hydraulic conductivity, K_i , sampled from the PDF, $Q_i = -K_i \cdot S \cdot \nabla h^*$.

The Monte Carlo technique was applied for 1000 runs using Simple Random Sampling. No Latin Hypercube Sampling was applied. The sampling was performed using MATLAB routines. The uncertainties of the material input data as defined by PDFs (marginal distributions) were implemented exactly as defined in the specifications of Benchmark 2. The degradation of the concrete in time/space was also implemented in accordance with the Benchmark 2. However, due to time constraint, correlations were only implemented in the case of parameters with normal and log-normal distributions; correlation coefficients in bold in Table 3.2-1 were implemented while correlation coefficients in strikethrough were not. All constraints defined in the Benchmark were implemented, but it was done in the following manner:

$K_{\text{micro-fissured zone}} > K_{\text{horizontal undisturbed argillites}}$

$K_{\text{fractured zone}} > K_{\text{micro-fissured zone}}$

If $K_{\text{micro-fissured zone}} \leq 10 K_{\text{horizontal undisturbed argillites}}$

then $De_{\text{micro-fissured zone}} = De_{\text{undisturbed argillites}}$

$De_{\text{micro-fissure}} > De_{\text{undisturbed argillites}}$

If $K_{\text{fractured zone}} \leq 10 K_{\text{horizontal undisturbed argillites}}$

then $De_{\text{fractured zone}} = De_{\text{undisturbed argillites}}$,

$De_{\text{fractured zone}} > De_{\text{micro-fissured zone}}$

If $K_{\text{micro-fissured zone}} \leq 10 K_{\text{horizontal undisturbed argillites}}$

then $\text{porosity}_{\text{micro-fissure}} = \text{porosity}_{\text{undisturbed argillites}}$,

$\text{porosity}_{\text{micro-fissure}} > \text{porosity}_{\text{undisturbed argillites}}$

If $K_{\text{fractured zone}} \leq 10 K_{\text{horizontal undisturbed argillites}}$

then $\text{porosity}_{\text{fractured zone}} = \text{porosity}_{\text{undisturbed argillites}}$

$\text{porosity}_{\text{fractured zone}} > \text{porosity}_{\text{micro-fissured zone}}$

$\text{porosity}_{\text{cation fractured zone}} > \text{porosity}_{\text{anion fractured zone}}$

Observe the different interpretation done in the cases where 'if' conditions were replaced by the strict condition '>' (7 out of 11 constraints).

Undisturbed argillites			Micro-fissured zone			Fractured zone		
	De	ω	K	De	ω	K	De	ω
Kv	0.85	0.55	0.40	0.35	0.25	0.35	0.30	0.25
	De	0.60	0.35	0.30	0.20	0.30	0.30	0.20
		ω	0.25	0.20	0.15	0.25	0.20	0.10
			K	0.85	0.55	0.85	0.75	0.55
				De	0.60	0.75	0.65	0.50
					ω	0.50	0.45	0.35
						K	0.85	0.65
							De	0.70

Table 3.2-1 : Correlated input parameters considered in the JRC calculations

The probabilistic transport calculations provide the molar rate of the radionuclides from each of the main barriers versus time for up to one million years. These results were subsequently post-processed by in-house developed MATLAB routines for the uncertainty and sensitivity analysis.

4 Uncertainty and sensitivity analysis tools and techniques

4.1 Uncertainty analysis

4.1.1 *Uncertainty analysis tools used*

The target of the uncertainty analysis is to characterize as well as possible the output variables selected in the study. For this task several numeric statistics and graphic tools are available. In the next subsections is a short description of the statistics and graphic tools used and the lessons learnt.

4.1.1.1 *Numeric statistics*

The numeric statistics used in this report may be classified in four groups: (i) central tendency statistics (mean and median), (ii) quantiles (sample minimum, 1%, 5%, 25%, 50% - median, 75%, 95%, 99% and sample maximum), (iii) dispersion statistics (standard deviation), and (iv) shape statistics (skewness coefficient and kurtosis). Albeit the sample minimum and maximum and the standard deviation were not mandatory, see section 2.2.1, they were provided by at least one of the participants. This set of numeric statistics allows a reasonably accurate description of the output variables. The formal definition of these statistics and their mathematical properties may be seen in PAMINA deliverable D2.1.B.2 [8].

4.1.1.2 *Graphic tools (time and non time-dependent)*

Three types of non time-dependent output variables are used: peak molar rates, time to peak molar rates and molar rates at specific times. Time-dependent output variables considered are the molar rates over time. The graphic tools used to describe non time-dependent output variables are the pdfs, cdfs and ccdfs; which are respectively the graphic estimates of the probability density function, the cumulative distribution function and the complementary cumulative distribution function. PAMINA deliverable D2.1.B.2 [8] provides a summary of the methods available to estimate pdfs and cdfs from a sample. The ccdf is obtained by subtracting 1 less the value of the cdf in each sampled value (they are complementary curves that contain essentially the same information).

Regarding the time dependent output variables, the way to deliver graphic information about them is to compute (a selection of) the numeric statistics described in section 4.1.1.1 at each

time considered and representing them versus time. Another interesting plot is the representation of the individual runs versus time.

4.1.2 Lessons learnt about UA tools and recommendations

After all the uncertain analyses calculations done in both benchmarks, the following lessons have been learnt:

- the convenience of providing simultaneously plots (ccdfs) and tables containing information about non time-dependent output variables,
- the convenience of providing plots containing the evolution of numeric statistics over time simultaneously with the evolution of individual runs for time-dependent output variables,
- the preference of using ccdfs over cdfs and pdfs.

Regarding the first conclusion, the ccdf (also cdfs and pdfs) summarises in a plot the whole information contained in a sample. Nevertheless, the need of using logarithmic scales due to the spread of the output variables over orders of magnitude makes necessary to provide also some exact numeric estimates in order to get accurate values of the quantiles or other numeric statistics needed.

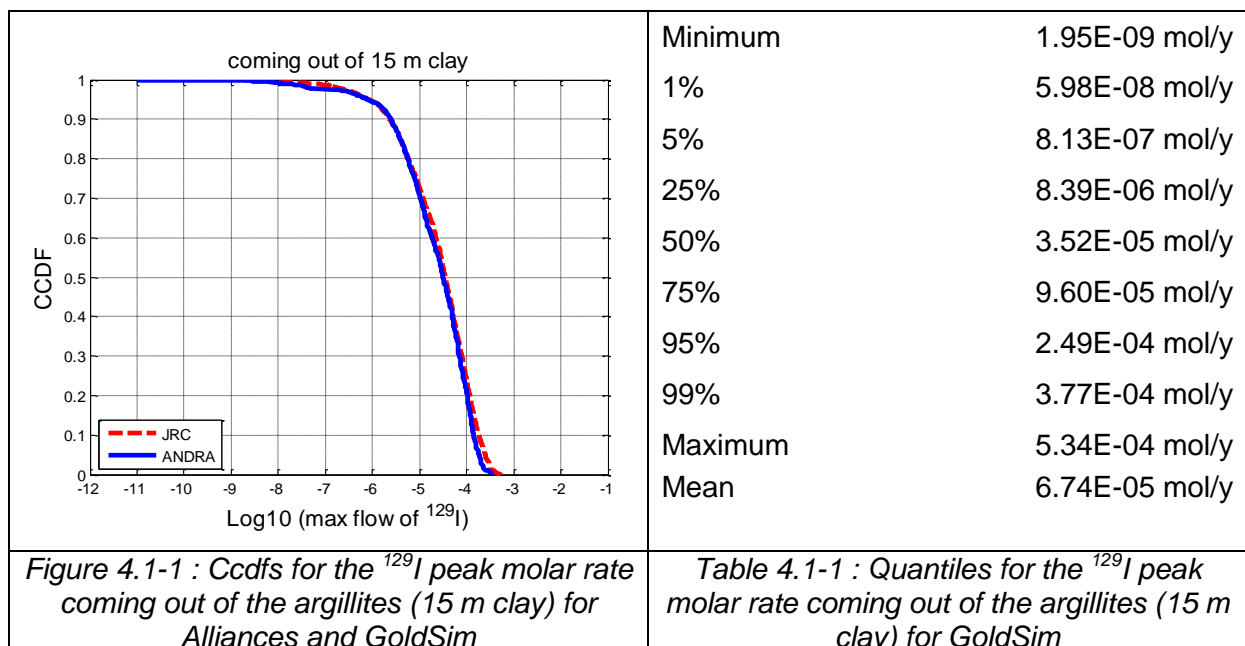
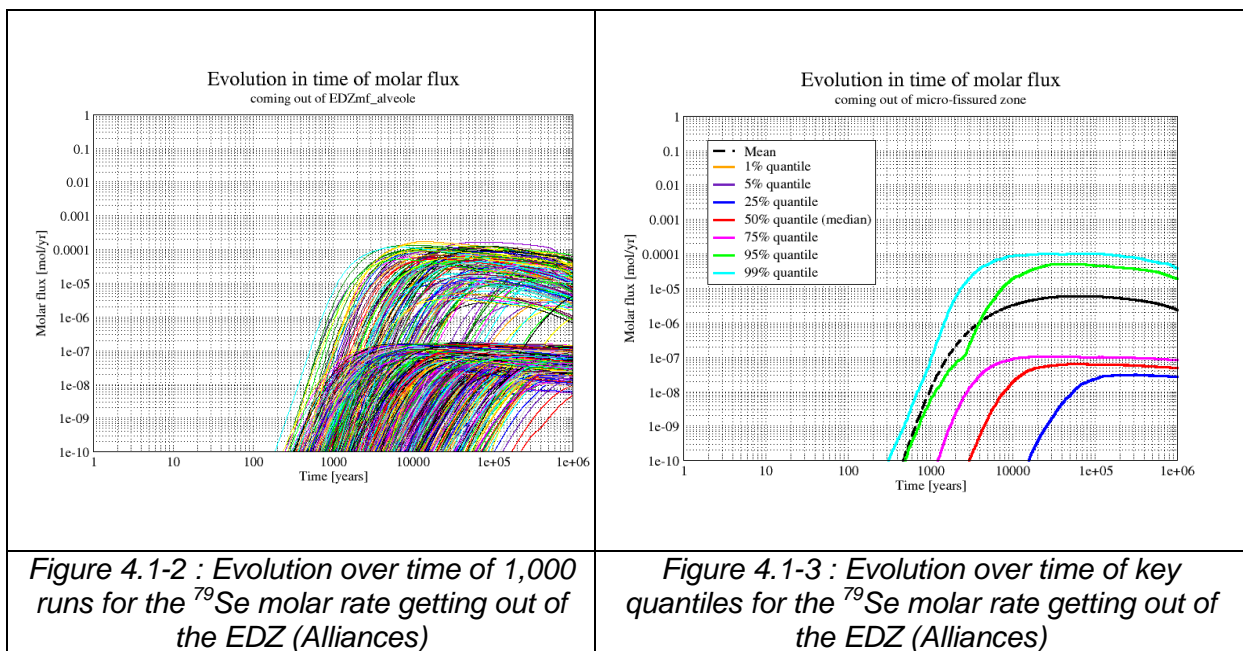


Figure 4.1-1 shows the ccdfs for the ^{129}I peak molar rates coming out of the undisturbed argillites (15 m clay) obtained by Andra and JRC. Table 4.1-1 contains the values of the selected quantiles for the ccdf obtained by JRC. Although the plot gives a very useful overview of the distribution of the variable represented, if an accurate estimate of the 95% percentile is needed, it is difficult to retrieve it from the plot, while Table 4.1-1 provides such accurate estimate ($2.49\text{E-}04 \text{ mol/y}$). Other values, such as the mean, would be unobtainable from the plot ($6.74\text{E-}05 \text{ mol/y}$).



The second conclusion applies to time-dependent output variables. Plotting key quantiles and other numeric statistics such as the mean and the standard deviation versus time provides very useful information to understand the time-dependent behaviour of the output variable. Nevertheless, it may hide relevant information that may be uncovered only if the individual runs are also shown, as the possible existence of sub-samples originated by the different behaviour of the system under different circumstances. This is the case shown in Figure 4.1-2 and Figure 4.1-3. These plots show respectively the evolution of the individual runs and of key quantiles for the ^{79}Se molar rate getting out of the EDZ obtained by Andra. The flat aspect of the curves corresponding to the 25%, the median and the 75% and the separation with respect to the curves corresponding to the upper quantiles may capture our attention and indicate that something peculiar is happening. Having access to Figure 4.1-2 helps understanding the existence of two sub-samples within the global sample with different upper bounds (a third sub sample does also exist but may not be detected because of the

lower bound used for the y-axis). Reviewing the input distributions and results of the sensitivity analysis will help understanding the connection of these results with the different values of the solubility limit distribution in the undisturbed argillites.

The last lesson learnt has to do with the preference of using ccdfs instead of pdfs and cdfs. Pdfs are very intuitive because they show the actual shape of the distribution showing what values are more likely and which are less likely (value of the ordinate). Nevertheless, it lacks all information about the quantiles (values that are exceeded with a given probability), which is very important in any safety related problem, as is the PA of a radioactive waste repository. The cdf provides for each value the probability of not exceeding it. This information is completely equivalent to the one contained in the ccdf (complementary to 1), but from the point of view of safety the latter is of more direct application.

4.2 Sensitivity analysis

The target of a sensitivity analysis (SA) is to identify which are the most important input parameters in a model and to understand the way they affect the output variables. In the following subsections is a summary of the SA techniques used in this study and the main lessons learnt.

4.2.1 Sensitivity analysis tools used

Three types of SA techniques have been used in this study: regression based statistics, Monte Carlo filtering statistics and graphic techniques.

4.2.1.1 Regression based statistics

Regression is a useful technique to study the relation between input parameters and a given output variable. When this SA technique is used, it is assumed that a kind of linear relation between input parameters and the output variable may exist; other relations are not accounted for. The main statistics associated to this technique are: the Pearson correlation coefficients (Pearson), the standardised regression coefficients (SRC) and the partial correlation coefficients (PCC). Pearson and SRC are exactly the same when the input parameters are independent. When input parameters are dependent all of them may be different from one another. A global measure of how good the linear model is to study the dependence between inputs and outputs is the coefficient of determination of the regression (R^2). More details about these techniques may be found in PAMINA milestone M2.1.D.4 [9].

When the R^2 is small, say below 0.6, the regression model may not be considered suitable to analyse the model. In that case two types of transformation may be of help: the logarithmic transformation and the rank transformation, see milestone M2.1.D.4 [9] for details. In the models studied in this work, the logarithmic transformation is not suitable for the molar rates over time because the output variable may take null values at different times, which makes impossible the use of this transformation. The rank transformation has been the only alternative. The rank transformation allows studying if a monotonic relation between inputs and output exists, whatever the monotonic relation might be. The equivalent regression statistics to Pearson, SRC and PCC are in this case, respectively, the Spearman rank correlation coefficient (Spearman), the Standardised Rank Regression Coefficient (SRRC) and the Partial Rank Correlation Coefficient (PRCC).

4.2.1.2 *Monte-Carlo filtering techniques (Mann-Whitney & Smirnov tests)*

In some cases, an input parameter could be considered important with respect to a given output variable if a clear link between specific regions of both exists. Monte Carlo Filtering (MCF) is based on dividing the output sample in two or more subsets according to some criterion (achievement of a given condition, exceeding a threshold, etc.) and testing if the inputs associated to those subsets are different or not. As an example, we could divide the output sample in two parts, the largest 10% results and the rest (rule 10%/90%). We could wonder if points in both subsamples are related to different regions of a given input or if they may be related to any region of that input. In the first case, knowing the value of that input parameter would be relevant to predict the value of the output, while in the second case it would not be. Two non-parametric statistics have been used in this work as MCF techniques: The Smirnov statistic (and associated test) and the Mann-Whitney statistic (and associated test), see reference [9] for further details.

4.2.1.3 *Graphic tools (scatter-plots, cobweb plots and CSM plots)*

Scatter-plots, cobweb plots and Contribution to the Sample Mean plots (CSM plots) have been the three graphic tools used in this work. Scatter-plots have been used by Andra while JRC has used cobweb plots and CSM plots.

Let us call $\mathbf{X}=(X_1, X_2, \dots, X_k)$ the vector of input parameters and Y to a given scalar output variable. For a given input X_i , the scatter-plot is the projection of the sample points (\mathbf{X}, Y) on the (X_i, Y) plane. This representation allows the examination of the dependence between Y and X_i . Scatter-plots are very helpful to identify linear relations, monotonic relations and the

existence of thresholds among other potential trends. The use of transformations may also provide a lot of information about input/output relations. The main shortcoming of this tool is that only one output versus one input may be represented per plot.

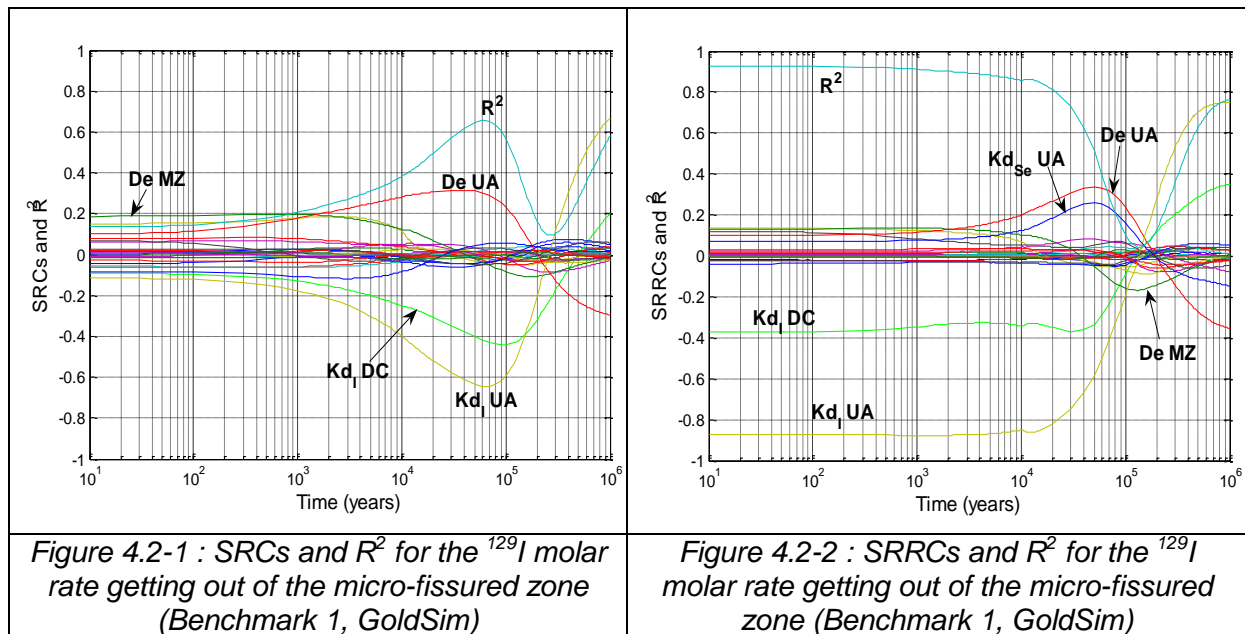
Cobweb plots have been designed to show multidimensional samples in a two-dimensional graph. Vertical parallel lines separated by equal distances are used to represent the sampled values of a given number of inputs/outputs, usually not more than ten or twelve, in order to keep the plot sufficiently clear. Each vertical line is used for a different input/output and either the raw values or the ranks may be represented (either raw values or ranks in all lines, never mixed). Sampled values are marked in each vertical line and jagged lines connect the values corresponding to the same run. Coloured lines can be used to display the different regions of any input parameter or output variable. Moreover, flexible conditioning capabilities enable an extensive insight into particular regions of the mapping. In fact, cobweb plots used in this work have always been conditional cobweb plots, where only the samples corresponding to a specific range of the output are represented (10% largest values always).

A CSM plot represents the fraction of an output variable sample mean that is due to any given fraction of smallest values of any input, see reference [10]. This reference does also provide a justification for the link between a CSM plot and first order sensitivity indices in a variance decomposition based SA.

4.2.2 Lessons learnt about SA tools and recommendations

4.2.2.1 Lessons learnt about regression techniques

Very poor quality results (small R^2) were obtained by both partners when working on the raw values. The quality dramatically increased when regressions were based on the ranks (of both, inputs and outputs). This scale (ranks), which is adequate to analyse monotonic relations, seems much more appropriate to study the data of both benchmarks than the linear scale. Figure 4.2-1 and Figure 4.2-2 show an example of this effect. See the differences in the values of R^2 and the SRCs and SRRCs in these two figures. Both represent the results of the linear regressions for ^{129}I in the micro-fissured zone in raw values and in ranks respectively. It can be observed the large difference in the value of R^2 , which measures the global quality of the regressions obtained.



The second lesson learnt has to do with the inclusion in the regression analysis of input parameters that a priori we know that cannot affect the output. This is the case, for example, of the Kd of Se in the undisturbed argillites ($K_{d_{\text{Se UA}}}$) in Figure 4.2-2. A priori we know that the behaviour of Iodine is completely independent of any parameter that affects only Selenium. Certainly the peak that SRRC obtains close to 50,000 years is an artifact of the data that has no theoretical support. This was observed in benchmark 1 and, as a conclusion of this benchmark, this type of input parameters were excluded from the analysis in benchmark 2. In general, the advice is not to include this type of input parameters in the analysis in order to avoid spurious SA estimates.

The third lesson learnt has to do with the following phenomenon, which was observed several times: a given input parameter strongly correlated with the output (responsible for a large fraction of the output variability) switches sign at a given time (from positive to negative or vice versa). This fact produced a dramatic drop in the value of R^2 at the time of the sign switch. Figure 4.2-2 shows this effect. The SRRC associated to $K_{d_{\text{I UA}}}$ (Kd of Iodine in the undisturbed argillites layer) changes sign around 10^5 years; before that time it is close to -0.9 and after that time reaches a value close to 0.8 . Observe the strong correlation between the mentioned SRRC and R^2 .

In principle, the regression model used could be considered appropriate to study the system at all times except around 10^5 years, because R^2 is quite large except around that time. Nevertheless, the regression model may be considered appropriate at all times because the

drop in R^2 is a simple consequence of the SRRC sign switch. When two variables are strongly positively (negatively) correlated at early times and strongly negatively (positively) correlated at late times, the only possibility is that in the mean time the relation between them becomes non-monotonic (non-linear). Taking this into account, the analyst concludes that that input parameter is important at all times, not only when the absolute value of the SRRC is large. Even when R^2 is not large, enough information is obtained from the data to understand the system behaviour, which makes the SA technique used appropriate.

4.2.2.2 *Lessons learnt about scatter-plots, cobweb plots and CSM plots*

The three graphic SA representations used in this work have shown their power and usefulness to understand the model behaviour. They are all complementary and provide different perspectives about the data analysed. The following lessons have been learnt about these tools along this application:

- Scatter-plots have shown their usefulness to retrieve information about model behaviour, specially using the logarithmic transformation, when it was possible, which suits better the simulation data.
- Cobweb plots have been identified as a very effective tool to support graphically the results obtained via MCF techniques. The results of the Man-Whitney and Smirnov tests (a p-value) are not physically intuitive. The following procedure for a given output variable helps understanding the results provided by the two statistics:
 - Perform both tests and select the input parameters that arise as important (low p-value)
 - Generate the cobweb plot for only those input parameters
- CSM plots provide very interesting information about the different contribution to the mean of the output variable of different regions of each input parameter. Only parameters that result in a rejection of the null hypothesis (at least one point outside the band parallel to the diagonal) should be represented.
- Cobweb plots and CSM plots are preferred to scatter-plots because they provide much more information in one single plot (several input parameters per plot).

4.2.2.3 Lessons learnt from the simultaneous use of different SA techniques

Both organizations have used simultaneously different techniques in both benchmarks, although this has been most remarkable in the second one. Two main lessons learnt may be highlighted:

- The use of different techniques (numeric and graphic) allow to get different pieces of information about the system under study, which helps understanding the system.
- A large degree of agreement has been systematically obtained among the different techniques, particularly regarding the most important parameters.

Table 4.2-1 shows a part of the results (only the most important parameters are shown) obtained by JRC in benchmark 2 for the ^{129}I peak molar rate at the second radial surface via regression analysis and MCF. Figure 4.2-3 and Figure 4.2-4 show the cobweb plot and the CSM plot for the same case. Results represented in Table 4.2-1 for Smirnov and Mann-Whitney are the p-values of the corresponding tests (the lower the p-value the more important the parameter), while for SRRC the value reported is the statistic itself. The value in parenthesis is the importance order. As it can be seen, the degree of agreement is remarkable; only Mann-Whitney provides a slightly different ordering of input parameters, but the tiny value of the p-values must be taken into account.

	Smirnov	Mann-Whitney	SRRC	R²
Kd _{DC}	1.81E-42 (1)	1.33E-39 (2)	-0.923 (1)	0.968
DeFZ	9.52E-04 (3)	4.24E-03 (3)	0.108 (3)	
Kd _{UA}	1.00E-34 (2)	0.0 (1)	0.313 (2)	

Table 4.2-1 : Most important SA results obtained by JRC in benchmark 2 for the ^{129}I peak molar rate at the second radial surface via regression analysis and MCF

The same degree of agreement may be observed when comparing these numeric results with the cobweb plot and the CSM plot (Figure 4.2-3 and Figure 4.2-4 respectively). The cobweb plot shows the relation between the largest values of the output and the largest values of Kd_{UA} and the smallest values of Kd_{DC}. Additionally, the CSM plot shows the same order of importance given by Smirnov and SRRC. Moreover, this plot shows

information not provided by any other one, as for example that the 10% largest values of $K_d|DC$ hardly have any impact on the output mean. The CSM plot does also show the agreement with the SRRC regarding the sign of the correlation (negative – above the diagonal; positive – below the diagonal). The general agreement among different techniques has been observed along the whole study.

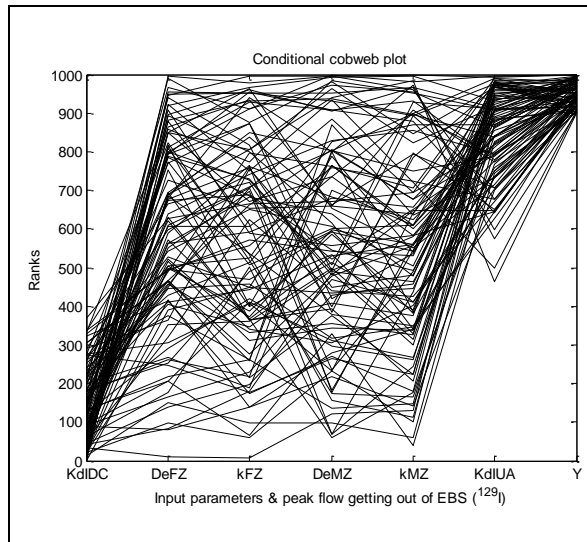


Figure 4.2-3 : Cobweb plot for the ^{129}I peak molar rate at the second radial surface (Benchmark 2, GoldSim)

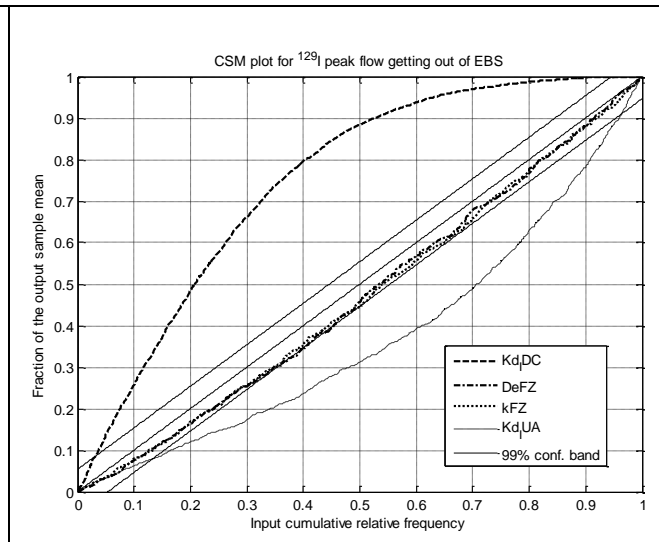
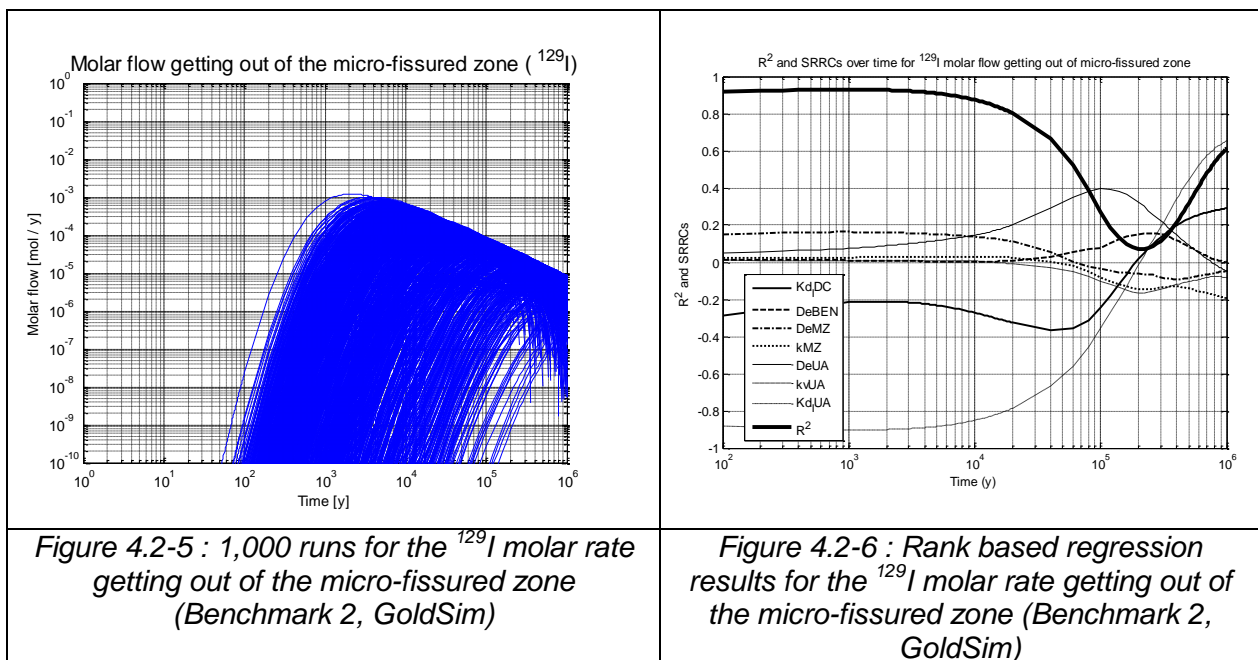


Figure 4.2-4 : CSM plot for the ^{129}I peak molar rate at the second radial surface (Benchmark 2, GoldSim)

4.2.2.4 Lessons learnt about the simultaneous use of UA and SA to improve system understanding

The simultaneous use of UA tools and SA techniques may help a lot understanding the way the system works, by means of explaining why SA techniques are delivering some specific results. Figure 4.2-6 shows the rank based regression results for the molar rate of ^{129}I getting out of the micro-fissured zone. These results are equivalent to the ones shown at the beginning of section 4.2.2.1 (Figure 4.2-2), which were obtained in benchmark 1. In Figure 4.2-6 the SRRC associated to $K_d|UA$ is negative and large at early times and becomes positive and large at late times; at around 200,000 years it is null and changes sign, from negative to positive. This change of sign of the most important input parameter in this layer produces the already mentioned (section 4.2.2.1) drop in the R^2 . The reason for this change of sign is in Figure 4.2-5. In this figure we can see that the different runs are shifted in time; some runs produce large molar rates quite early while others are very delayed (some runs

appear in the picture before 100 years while others appear as late as 100,000 years). We can also see that runs that produce very large molar rates at early times generate low molar rates at late times and vice versa. Figure 4.2-6 indicates that large early molar rates are related to small values of $K_d|_{UA}$, while large late molar rates are related to small large values of $K_d|_{UA}$. The drop in the R^2 and the change of sign of the SRRC associated to $K_d|_{UA}$ is due to the crossing of runs around 200,000 years; early runs that peaked very high are decreasing and cross runs that are very delayed, still growing.



5 Simulation results and comparison

5.1 Results from benchmark 1 – Comparison 1D/2D

Benchmark 1 was the first step in the process to benchmark complex (Andra) and less complex (JRC) models. It was also the opportunity to apply a fully developed probabilistic test case. The degree of agreement between both partners was really remarkable. The molar rates in the different parts of the system computed by JRC and Andra were very similar except for the peak value in the waste package and disposal cell. Figure 5.1-1 and Figure 5.1-2 show the results provided by both partners for the ^{129}I molar rate getting out of the waste packages; see the remarkable agreement except for the height of the peak at 10,000 years. This peak value is caused by the stepwise change in the concrete properties at 10,000 years, which gives a very high peak but with a short duration. Andra has a higher peak value because it has a much finer time discretisation around this event. Figure 5.1-3 and Figure 5.1-4 show the same results obtained by both partners for the ^{129}I molar rate getting out of the undisturbed argillites (15 m from the centre of the disposal cell); both results are very close to one another.

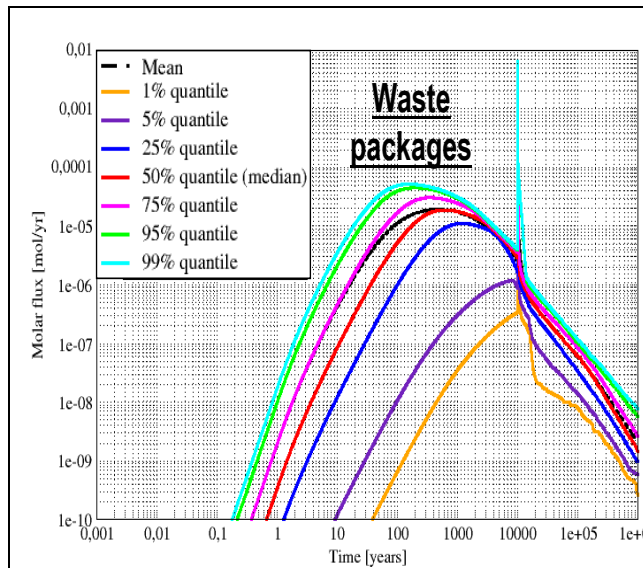


Figure 5.1-1 : Evolution over time of ^{129}I molar rate getting out of the waste packages (key quantiles, Benchmark 1, Alliances)

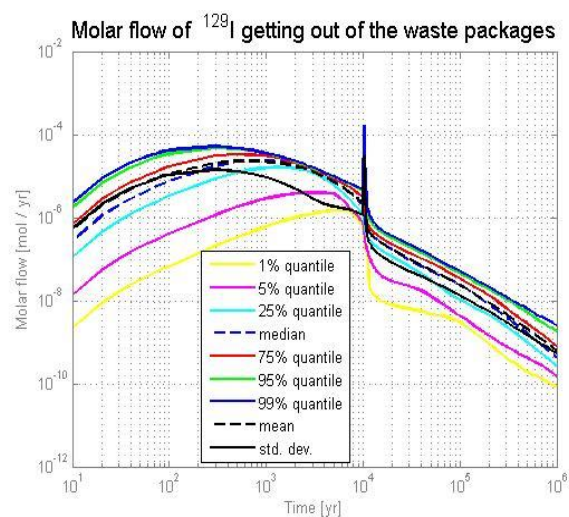
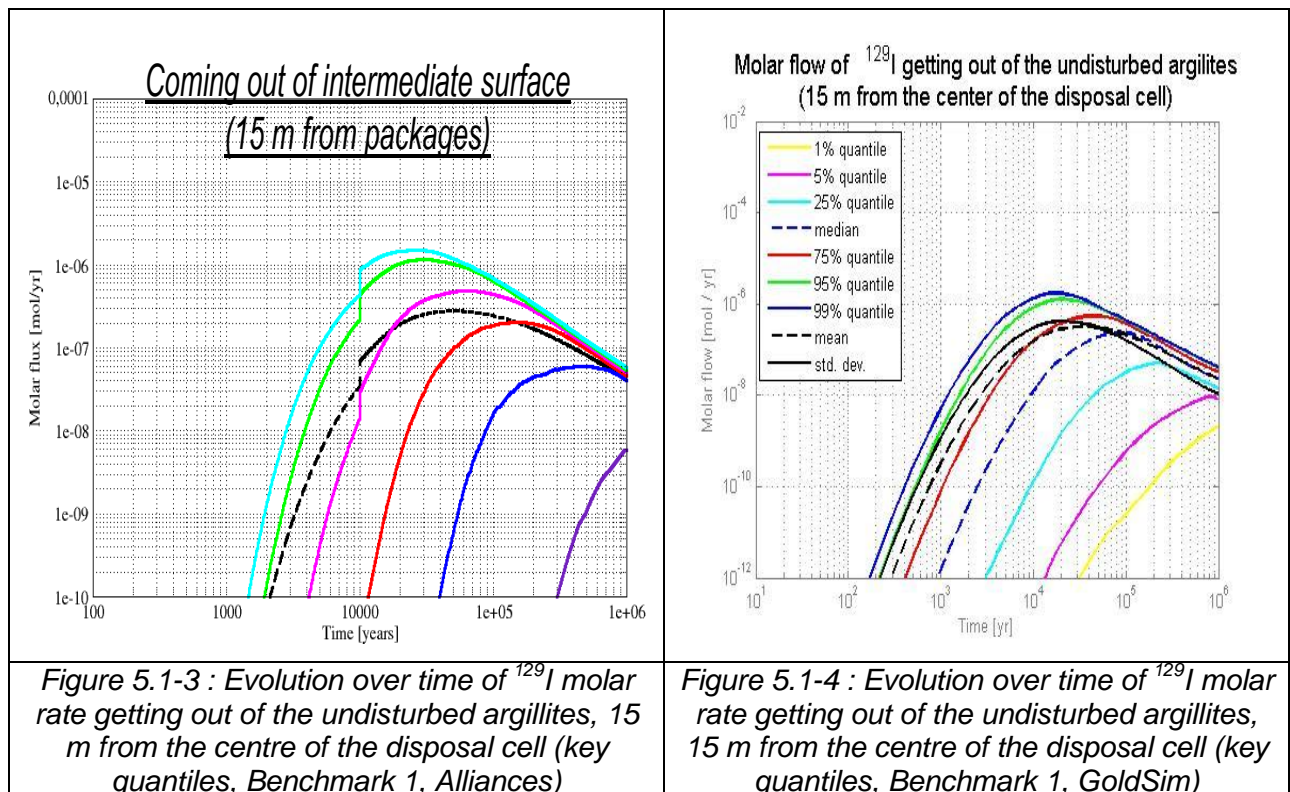


Figure 5.1-2 : Evolution over time of ^{129}I molar rate getting out of the waste packages (key quantiles, Benchmark 1, GoldSim)

The computed sensitivity standardised rank regression coefficients with respect to the molar rate for key input parameters were also similar when plotted versus time. There was a large difference though when looking at the peak molar rate out of the waste package and the disposal cell because of the already mentioned difference in the time discretization at 10,000 years.



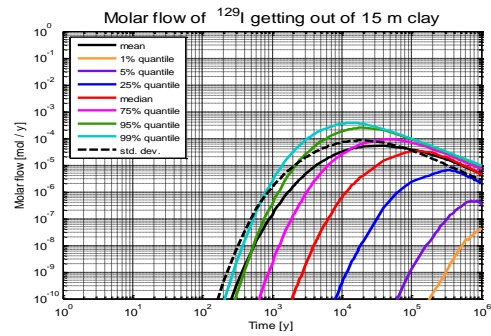
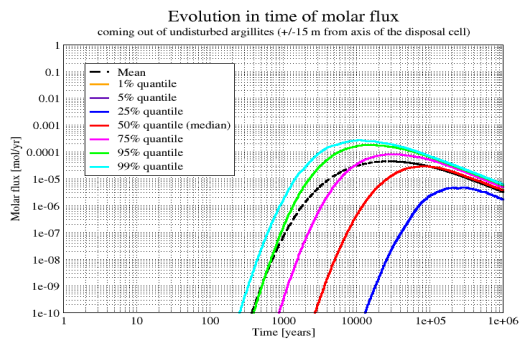
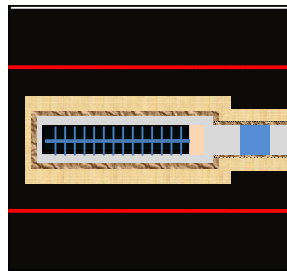
Andra's model is much more complex than JRC's in terms of geometrical description, transport processes and parameter constraints. The good agreement in results (except for the peak) between the more complex Andra and the simpler JRC analysis is because the molar rate is diffusion controlled: the distribution coefficient (Kd) and the effective diffusion coefficient (De) control the molar rate out of the clay layer.

5.2 Results from benchmark 2 – Comparison 2D/3D

Before comparing the results from Andra and JRC we summarize the main differences in the modelling: Andra (Alliances) models all aspects described in the benchmark; it is a complete 3D-model with all the transport modes included and all correlations and constraints implemented. Andra (Alliances) uses Latin Hypercube Sampling (LHS) with the constraints imposed. JRC (GoldSim) uses a 2D cylindrical geometrical description, with an advective flow rate (in the form of Darcy velocities) calculated on the basis of Alliances hydraulic results provided by Andra for a particular case (reference most probable case). Correlations are implemented only in the case of parameters with normal and log-normal distributions and 7 out of the 11 constraints are implemented replacing the 'if' conditions by the strict condition '>'. JRC used Simple Random Sampling (SRS) since it allows accounting for constraints in a strict sense.

In spite of the rather large difference in the level of complexity in radionuclide migration, the computed molar rates are quite similar for the **radial pathway** for ^{129}I . This confirms the conclusions drawn from the first benchmark that if we only consider the hostrock pathway then the simpler geometrical model is adequate. This can be seen in Figure 5.2-1 and Figure 5.2-2, which show the comparison of quantiles of molar rates for Alliances and GoldSim in undisturbed argillites at 15 m and 65 m from the waste packages (top and bottom of clay layer), whereas Figure 5.2-3 depicts the comparison of complementary cumulative distribution function (ccdf) for the two output surfaces. Despite the differences in correlations and constraints implementation, we observe quite a good agreement between Alliances and GoldSim results for this pathway (quantiles curves and ccdf's curves are very similar). The reason is that diffusion is the predominant transfer mode, which is also modelled accurately in the simplified JRC analysis, and that the two codes use the same data for the distribution functions for the relevant input parameters.

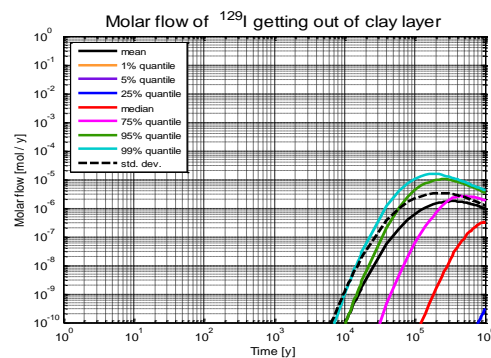
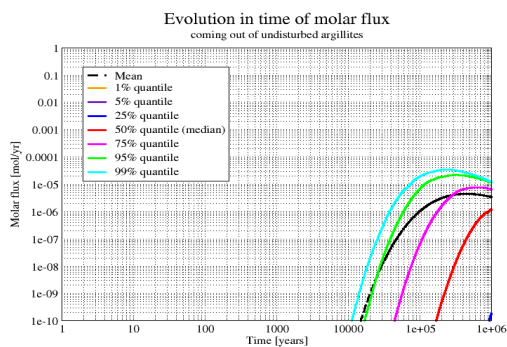
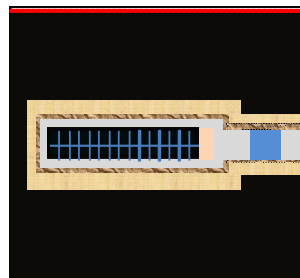
Table 5.2-1 gives the three most important rank indicators for the peak molar rate out of the disposal cell and out of the undisturbed argillites in the radial direction and into the gallery in the longitudinal direction. There is clearly a good agreement. The distribution coefficient in the concrete and the undisturbed argillites are the most important indicators for both Andra and JRC. Hence for ^{129}I in the host rock pathway we conclude that there is good agreement between the two sets of analyses both with respect to uncertainty analysis and sensitivity analysis.



a)

b)

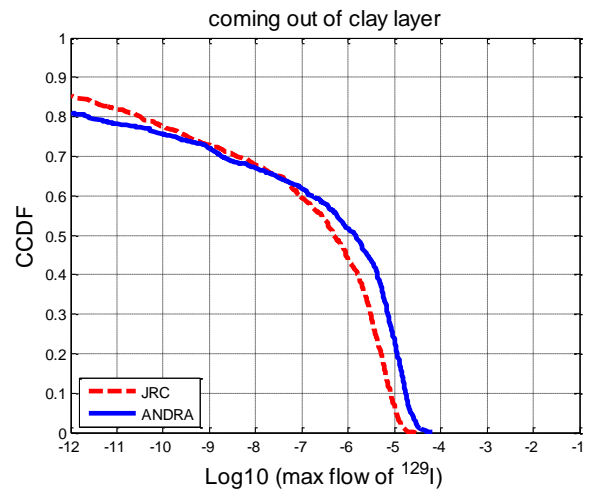
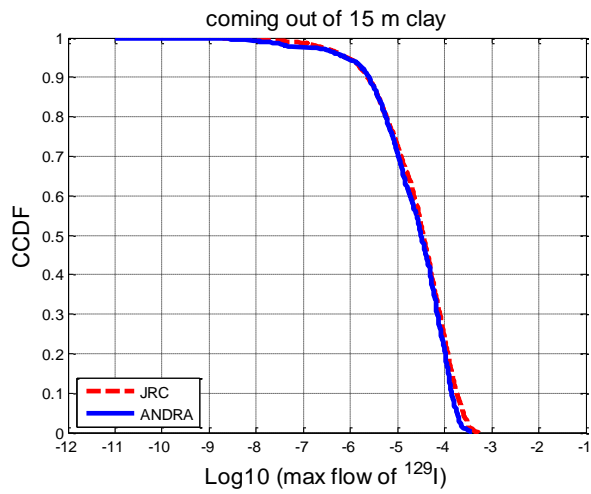
Figure 5.2-1 : Alliances/GoldSim comparison of quantiles of molar rates getting out of 15 m within clay in the case of ^{129}I : a) Alliances and b) GoldSim



a)

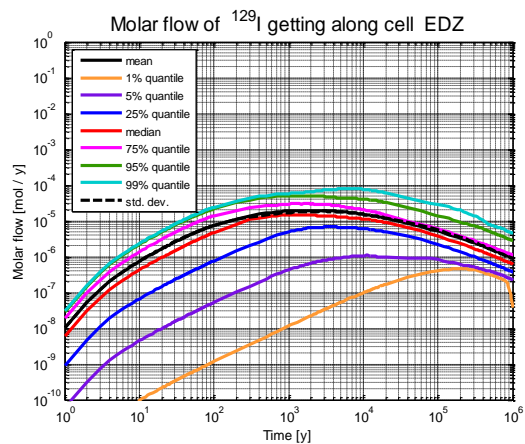
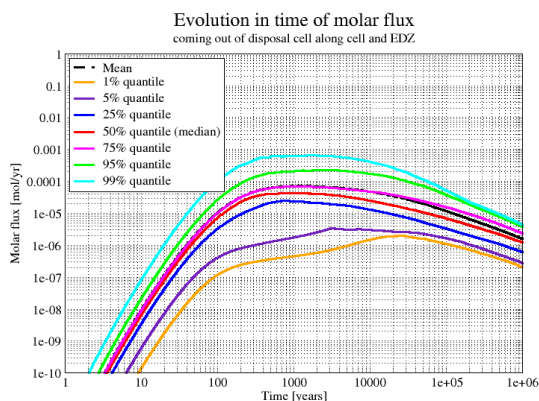
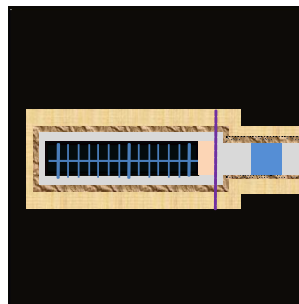
b)

Figure 5.2-2 : Alliances/GoldSim comparison of quantiles of molar rates getting out of the clay layer (top and bottom) in the case of ^{129}I : a) Alliances and b) GoldSim

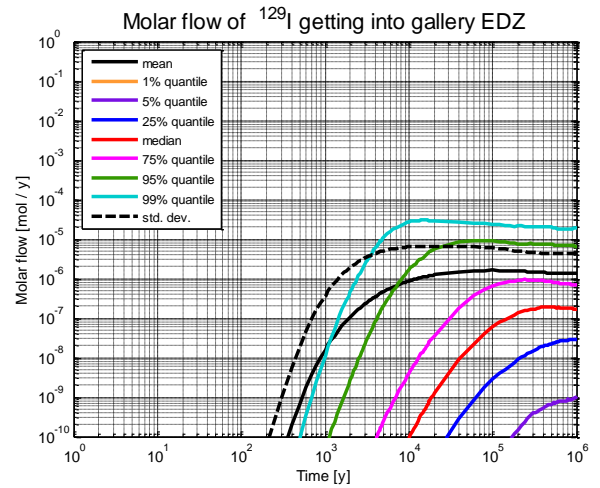
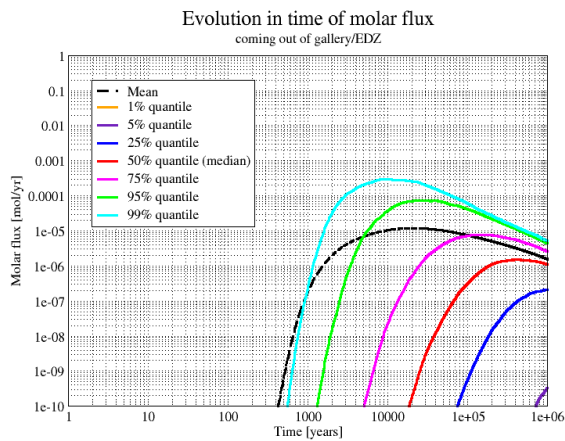
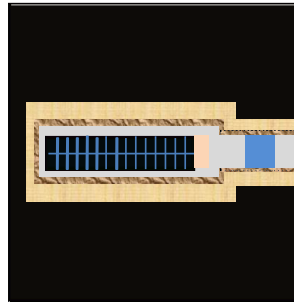


a) b)
 Figure 5.2-3 : Alliances/GoldSim comparison of ccdf in the case of ^{129}I : a) out of 15 m clay and b) out of clay layer

The quantiles out of disposal cell along cell/EDZ and out of gallery/EDZ for the **axial pathway (^{129}I)** are depicted in Figure 5.2-4 and Figure 5.2-5 respectively whereas Figure 5.2-6 shows the associated cdfs.



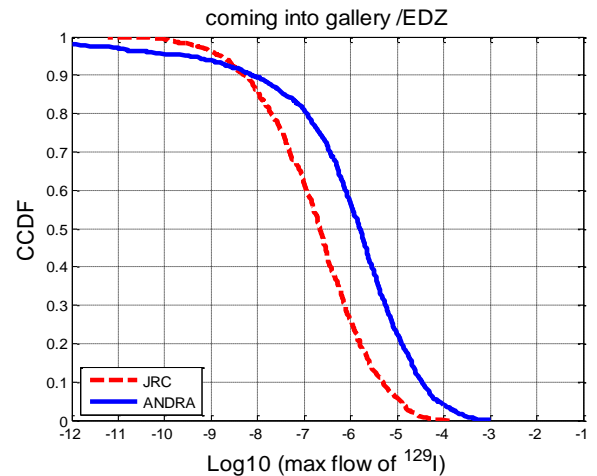
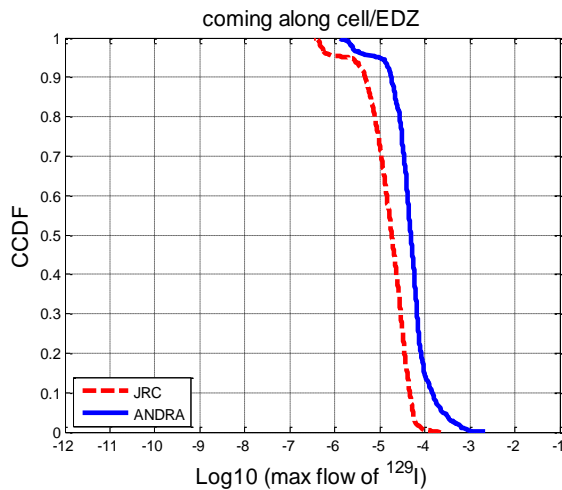
a) b)
 Figure 5.2-4 : Alliances/GoldSim comparison of quantiles of molar rates getting out of disposal cell along cell/EDZ in the case of ^{129}I : a) Alliances and b) GoldSim



a)

b)

Figure 5.2-5 : Alliances/GoldSim comparison of quantiles of molar rates getting out of gallery/EDZ in the case of ^{129}I : a) Alliances and b) GoldSim



a)

b)

Figure 5.2-6 : Alliances/GoldSim comparison of ccdf in the case of ^{129}I : a) out of disposal cell along cell/EDZ and b) out of gallery/EDZ

For this second pathway, the peak values and to a lesser extent the shape of the quantile curves appears to be similar, but we observe some differences on the levels of molar rates and the transfer times. The larger discrepancy between the Andra and JRC analyses for the longitudinal pathway compared to the radial pathway is expected since the influence of the advective pathway is no longer negligible. As explained above for the advective pathway, GoldSim does not take into account explicitly the link between the hydraulic conductivity of each sample and the water flow drained by the disposal cell, which controls the advective pathway within and along the disposal cell. Water flow within GoldSim is actually constant for each sample, and identical for all cells describing the disposal cell. This topic highlights two limitations regarding the use of codes such as GoldSim for probabilistic 3D studies. First of all, each simulation requires in principle that a preliminary 3D hydraulic calculation has to be systematically performed in order to “feed” each GoldSim cell with flow rates. This would definitely request a huge amount of work, similar to running many 3D simulations with a numerical tool, that are consistent with the space discretization. Such a calibration would be highly time consuming and onerous. Secondly, a link between the water flow and the hydraulic conductivity of undisturbed argillites was defined for each run through the hydraulic gradient. However, the full 3D problem is more complex, since the advective kinetic is linked to many hydraulic conductivities (undisturbed argillites, fractured zone, micro-fissured zone, ...) and not only one, and also to the head gradient which varies along the disposal cell. The set-up of such a correlation is not feasible (non linear), considering all the possible combinations for input parameters.

The most important rank indicators for the peak molar rate into the gallery in the longitudinal direction are also given in Table 5.2-1. It can be noted that in the Andra analysis the vertical permeability is the most important parameter but it does not show up at all in the JRC analysis due to how advection was implemented by JRC. The distribution coefficient is included as an important parameter in both analyses. The contribution to the total variability is given by the square of the rank indicator ($\sum_{i=1}^k SRC_i^2 = R^2$, where k is the number of input uncertain parameters considered), which gives an even stronger dominance for the large indicators. In the radial direction there is always one parameter which dominates the variance whereas for the longitudinal rate there is no such leading parameter. This illustrates the much larger complexity of the longitudinal rate. Hence for the molar rate of ^{129}I along the disposal cell pathway we conclude that there is a reasonable agreement for the uncertainty analysis. It must be kept in mind though that the JRC analysis relied on input from the 3D

analyses by Andra. For the sensitivity analysis there is not much agreement which indicates that the feeding of 3D results to the cell model is not adequate.

Out of Disposal Cell (radial)		Out of Undisturbed Argillites (radial)		Into Gallery (longitudinal)	
GoldSim	Alliances	GoldSim	GoldSim	Alliances	GoldSim
$K_d(\text{concr}) = -0.79$	$K_d(\text{concr}) = -0.92$	$K_d(\text{clay}) = -0.66$	$K_d(\text{clay}) = -0.89$	$K_v(\text{clay}) = 0.6$	$K_d(\text{clay}) = -0.61$
$De(\text{FZ}) = 0.33$	$K_d(\text{clay}) = 0.31$	$De(\text{clay}) = 0.26$	$De(\text{clay}) = 0.39$	$K_d(\text{FZ,clay}) = -0.5$	$K(\text{MFZ}) = 0.59$
$K_d(\text{clay}) = 0.22$	$De(\text{FZ}) = 0.1$	$K_d(\text{clay}) = 0.13$	$K_d(\text{concr}) = -0.1$	$K(\text{FZ}) = 0.44$	$De(\text{clay}) = -0.2$

Table 5.2-1 : The three most important rank indicators and their values for the ^{129}I peak molar rate at three interfaces

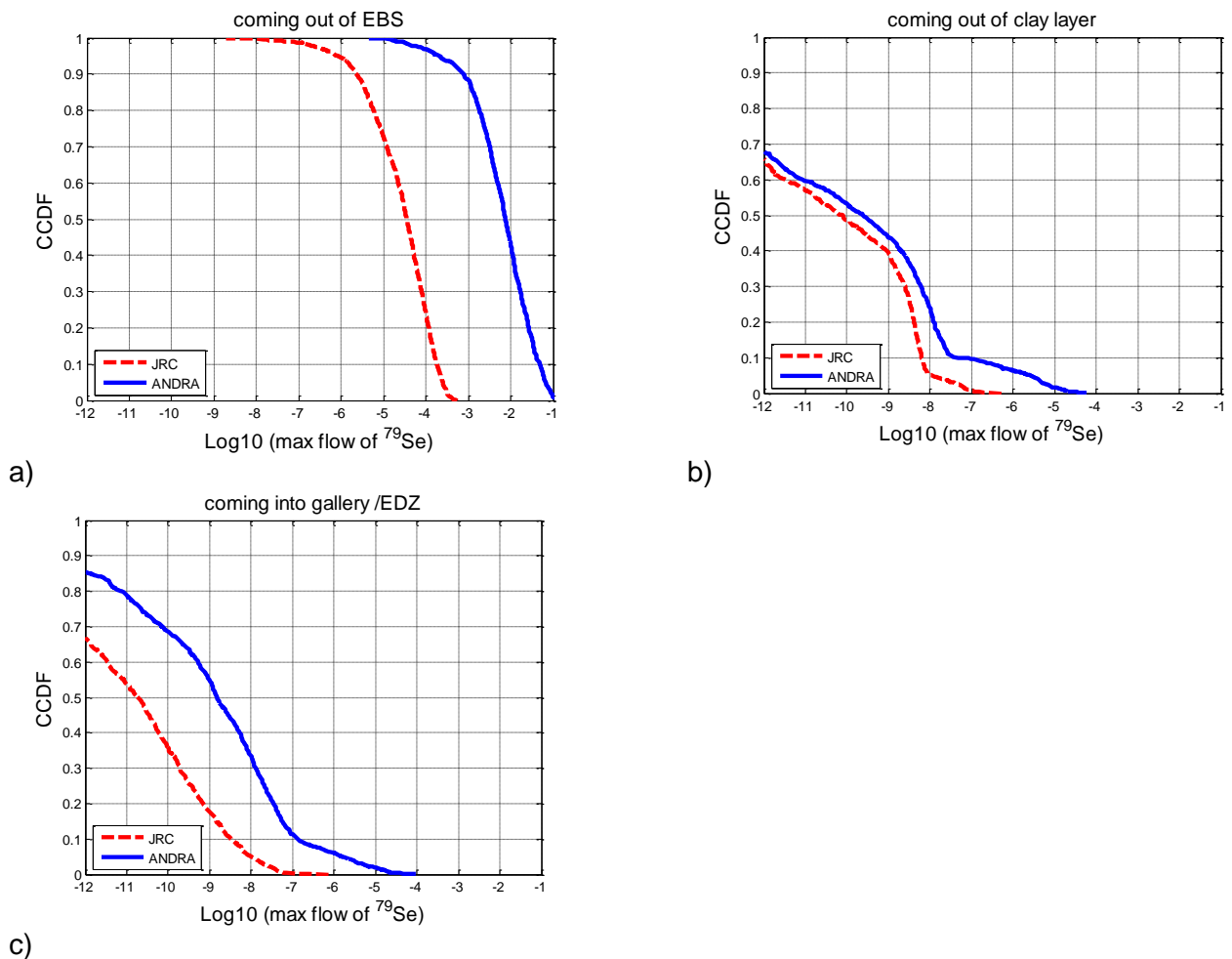


Figure 5.2-7 : Alliances/GoldSim comparison of ccdf for ^{79}Se : a) out of disposal cell in the host rock pathway ; b) out of the clay in the host rock pathway and c) out of gallery/EDZ in the longitudinal pathway

For ^{79}Se the differences between Alliances and GoldSim are larger than for ^{129}I . For both the radial and longitudinal directions Alliances gives generally higher molar rates. For the radial rate the difference is much larger out of the disposal cell than out of the clay layer 65 m from the waste package as seen in Figure 5.2-7 a) and b). The difference between Alliances and GoldSim predictions are also larger for the rate into the gallery than out of the clay layer as seen by comparing Figure 5.2-7 b) and c).

It is worth mentioning in this context that the radial rate in Benchmark 2 is higher than in Benchmark 1 for both Andra and JRC and that the difference between the two benchmarks are much larger out of the disposal cell than out of the clay layer (see Table 4.1-2 and Table 4.2-2 of M4.3.5 for Andra and JRC respectively). It can also be noted that the difference between the benchmarks is much smaller for JRC than for Andra. The difference between the Andra and the JRC analyses affects also the sensitivity analysis. This should be reflected in the ranking of the most important parameters shown in Table 5.2-2. The difference for the radial rate is, however, not so large: out of the clay layer Andra and JRC both identify the distribution coefficient and the diffusion coefficient as the most important parameters but the agreement for the parameters out of the disposal cell is surprising given the huge difference in the molar rate. For the longitudinal molar rate there is not a good correlation, which could be expected given the difference between the models.

Out of Disposal Cell (radial)		Out of Undisturbed Argillites (radial)		Into Gallery (longitudinal)	
Alliances	GoldSim	Alliances	GoldSim	Alliances	GoldSim
K_d (s.con) = -0.82	K_d (s.con) = -0.80	K_d (clay) = -0.58	K_d (clay) = -0.76	C_{sat} (clay) = 0.59	K (MFZ) = 0.48
C_{sat} (d.con) = 0.28	C_{sat} (clay) = -0.28	C_{sat} (clay) = 0.48	De (clay) = 0.39	K_v (clay) = 0.48	K_d (clay) = -0.39
C_{sat} (clay) = -0.26	K_d (d.con) = -0.15	De (clay) = 0.26	C_{sat} (clay) = 0.30	K (FZ) = 0.35	K_d (s.con) = -0.32

Table 5.2-2 : The three most important rank indicators and their values for the ^{79}Se peak molar rate at three interfaces

It is not clear why the difference in molar rate is so much larger for ^{79}Se than for ^{129}I . Possible explanations should be sought in the difference in the modelling other than geometry. One difference is that Andra assumed that the concrete within the waste disposal package zone had no sorption whereas JRC assumed the sorption had the value of the sound concrete up to 1 million years. The absence of sorption should give higher values for the peak molar rate out of the disposal cell but should have a small effect out of the clay, which is in line with the observations. Another potential source is that JRC did not account for the correlations



involving porosity, which is an important parameter for a nuclide subject to chemical precipitation. A third potentially important difference is that Andra used Latin Hypercube Sampling with the constraints imposed, which leads to a clustering of the random samples in accordance with the constraints (i.e. along the line "x=y"). In the JRC sampling the samples were distributed so that only samples that fulfilled the constraints were used. The main difference between the benchmarks for the radial rate was the description of the waste package and the degradation of the concrete. This should have a large effect on the rate out of the disposal cell but a small effect out of the clay layer since the most important parameters are related to the clay properties. The JRC calculations out of the clay layer are quite similar between the two benchmarks whereas for Andra there is a larger difference.

6 Complementary/alternative technique : meta-models based on response surfaces

6.1 Main objective

Taking into account the increasing complexity of studies in both respects, phenomenological and geometrical (couplings, non-linearities, high number of cells, ...), the use of probabilistic methods such as Monte-Carlo can turn out to be complex and expensive in computational terms. Therefore, the sensitivity analysis must open itself to more refined techniques of variance analysis, supported by the creation of meta-models based on response surfaces. These techniques such as neural networks or Chaos polynomials are an efficient way to generate a large number of simulations at a relatively low cost, which is the main objective.

6.2 Description of the method (different steps)

Figure 6.2-1 illustrates the different steps of creation and validation of meta-models applied to the 3D test-case described section 2:

Step 1: definition of the model and of the calculation indicators,

Step 2: definition and production of the design of experiments,

Step 3: building of meta-models (neural networks and Chaos polynomials),

Step 4: verification/validation of meta-models,

Step 5: application of meta-models.

For this document, the aim is not to go into many details describing each step. Only an illustration of the validation process (part of the fourth step) and an example of application (fifth step) are given in the following sections (6.3 and 6.4).

The ultimate application of meta-models can be described as follows:

- to evaluate, through different indicators, the effect of input parameters uncertainties on the results according to two directions: (i) the uncertainty analysis by means of calculation of various uncertainty indicators giving the spectrum and characteristics of variation (distribution of the results), and (ii)

the sensitivity analysis aiming at identifying and ranking the influent parameters on the results.

- to use the meta-model to carry out several thousand simulations and thus, to be able to compare the sensitivity of the results linked to the sample size.

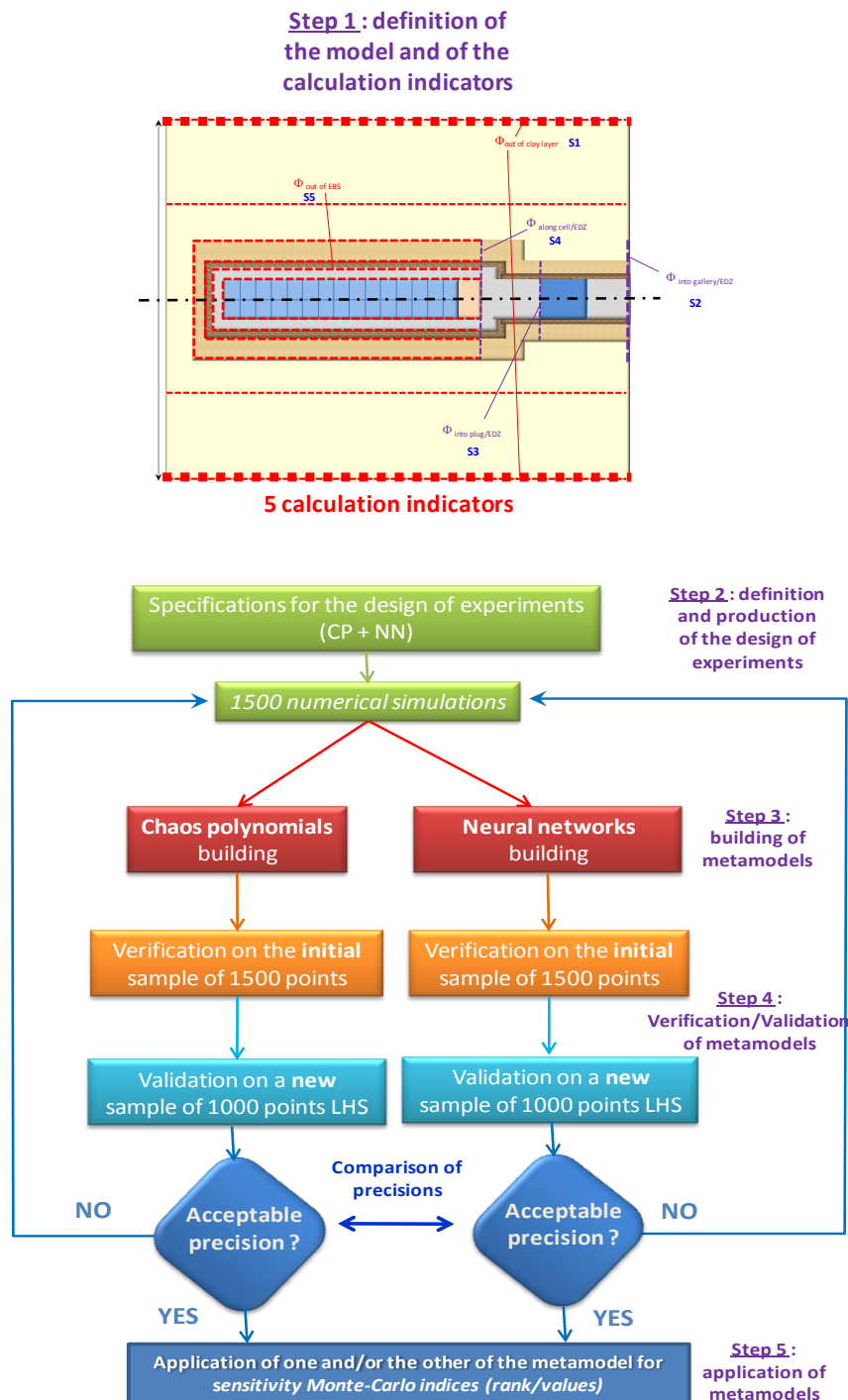


Figure 6.2-1 : Different steps of creation of meta-models

6.3 Validation step: comparison with Monte-Carlo/LHS simulations

Once the meta-models have been built, the verification step, not illustrated in this document, consists in applying the meta-models on the initial sample which has been used for building them (1,500 simulations in the present case). This has been done for both types of meta-models (neural networks and Chaos polynomials) for each indicator (maximum molar rate at each surface S_i , $i=1$ to 5).

The next step of validation, described and illustrated in this paragraph, is then carried out based on the definition of a new sample (1,000 Monte-Carlo LHS simulations in the present case). The results obtained from the 1,000 numerical simulations are compared to those provided using the meta-models for both types of meta-models and for each indicator. Figure 6.3-1 gives an illustration of such a comparison for the first indicator (maximum ¹²⁹I molar rate coming out of clay (surface S1)).

The results of the comparison are given analysing three indicators (the shape of scatter-plots, the R^2 determination coefficient of the model, the trend line linearity coefficient).

In the case of neural networks, the comparison (numerical model/meta-model) shows a very good prediction (focused scatter-plots on a large range variation). The value of R^2 determination coefficient (0.99) is very high (close to 1). The trend line linearity coefficient is also high ($y = 0.982 \cdot x$ close to the $y = x$ equation). Neural networks is thus a very promising technique.

In the case of Chaos polynomials, the scatter-plots show quite more dispersed results associated with a lower value of R^2 determination coefficient (0.26) and a lower value of the trend line linearity coefficient ($y = 0.391 \cdot x$, which is a bit far from $y = x$ equation). This highlights the great influence of the regularity of the sample for the Chaos polynomials method, but also the need to improve accuracy, whether it is by adding some iterations or increasing the polynomial degree.

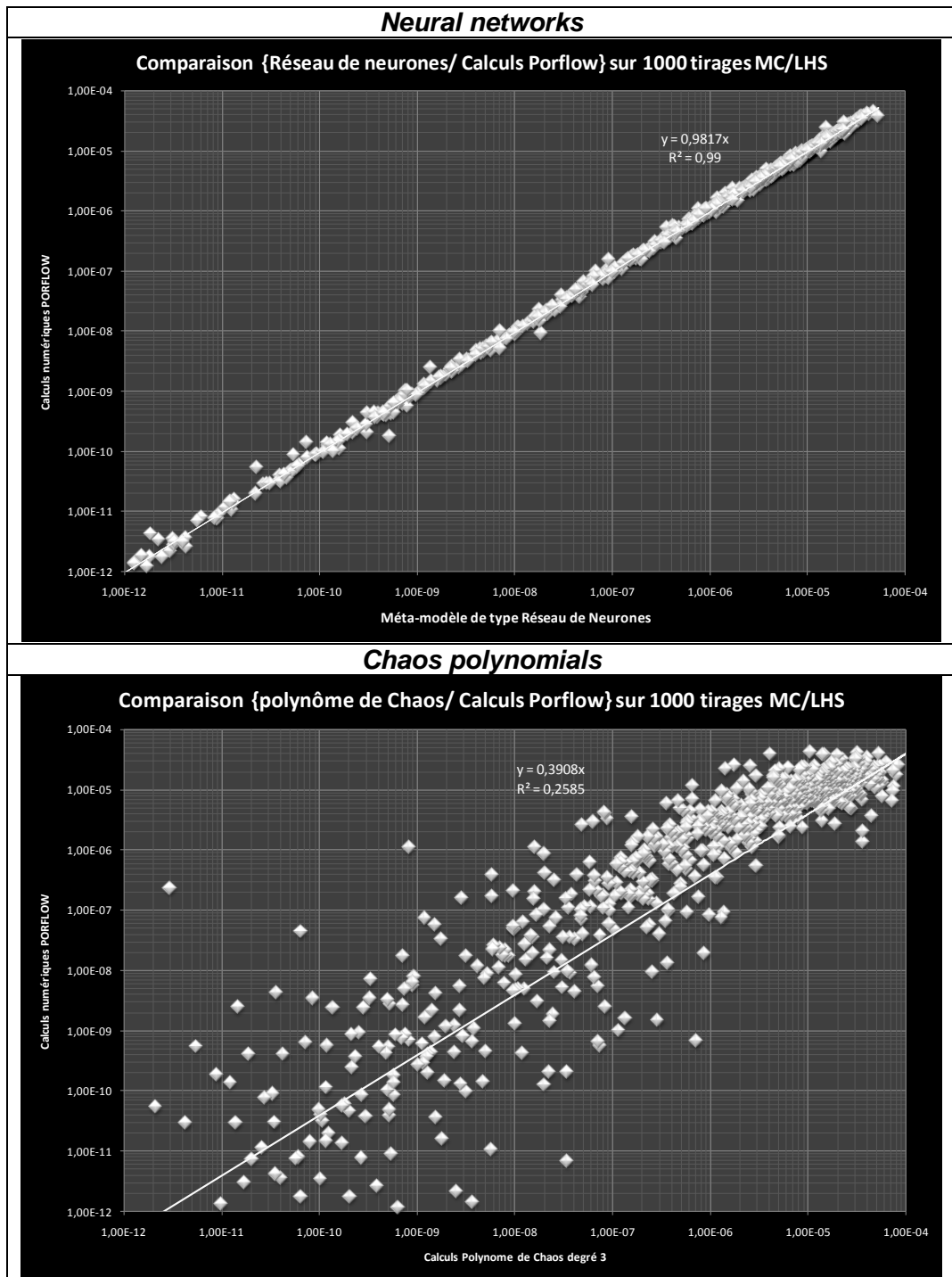


Figure 6.3-1 : Validation of meta-models (neural networks, Chaos polynomials) for the maximum ^{129}I molar rate coming out of clay

6.4 Example of application (neural networks): effect of sample size on the convergence and accuracy of estimates

One type of application illustrated in this paragraph is to use the meta-model to carry out several thousand simulations and to be able to compare the sensitivity of the results linked to the sample size (or number of simulations).

Figure 6.4-1 illustrates the effect of the sample size on the Spearman coefficient for the first indicator (maximum ^{129}I molar rate coming out of clay) and the two main influent parameters for this pathway (sorption and effective diffusion).

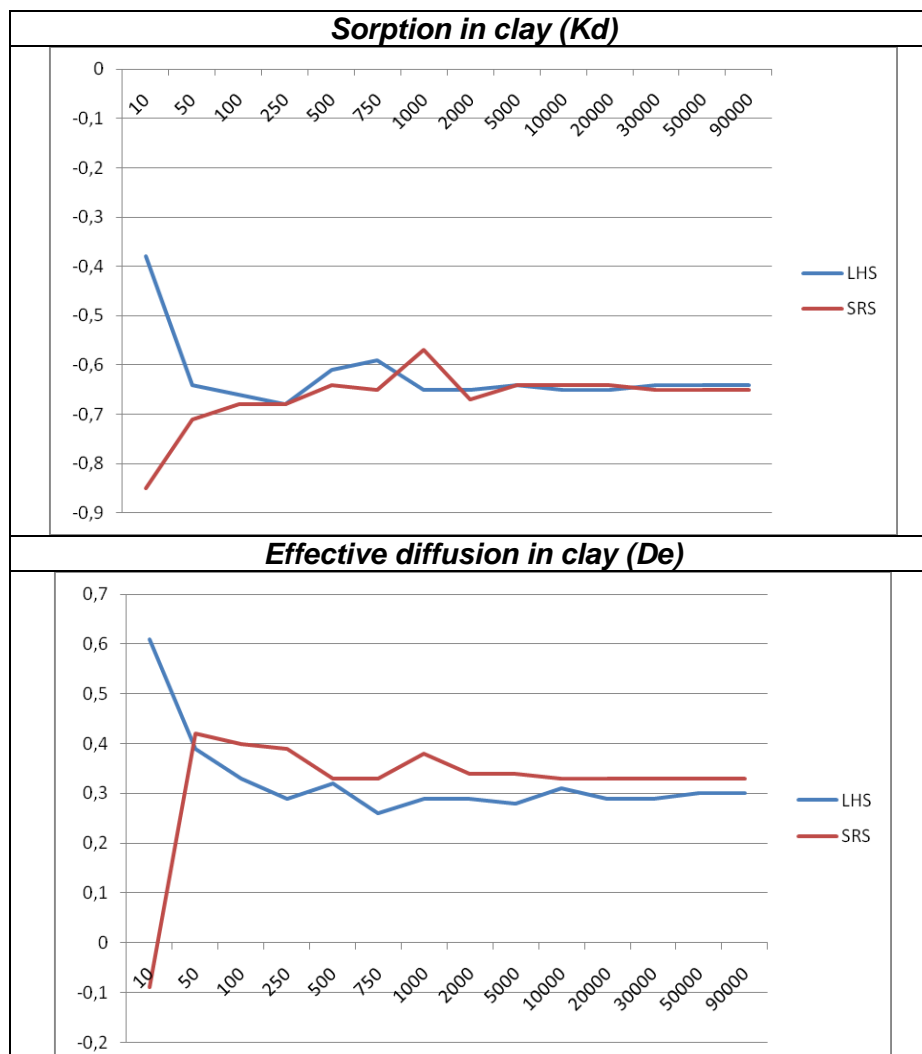


Figure 6.4-1 : Application of meta-models (neural networks): sensitivity to the sample size for the Spearman coefficient (for sorption and diffusion in clay)



The graph clearly shows that an optimum value for the number of simulations can be defined (between 2,000 and 5,000 in this case) over which the value of the Spearman coefficient remains quite stable. Nevertheless, 1,000 or 2,000 also appear to be quite acceptable values in terms of number of simulations (for PAMINA, we have carried out 1,500 numerical simulations which fits totally in the scope).

Another improvement initially foreseen but not performed within the PAMINA project, lies in the comparison of the Monte-Carlo rank-based and value-based indicators with the Sobol indices (more refined techniques of variance analysis).

7 General conclusions

Many interesting and useful results have been obtained whilst carrying out the two benchmarks in this joint study between Andra and JRC with the objective to apply advanced methods for uncertainty and sensitivity analysis of a clay repository. Two different tools have been used to perform the simulations: (i) the Alliances package used by Andra which allows a complex description of geometry and the processes, needed in order to take into account both pathways together in the case of the second benchmark (host rock and disposal cell pathways), and (ii) the GoldSim code used by JRC, which includes some simplifications in geometrical description and simplifications in the hydraulic processes. The analysis done was based on the Monte Carlo simulation technique which has been applied to the molar rates in different parts of the repository system as outputs. The input parameters that control the radionuclide migration in the analysis have been derived from the French research program on radioactive waste management. Thus, the application of this technique relies on a large data set derived from a detailed and comprehensive characterization program which has led to the set-up of pdfs for 40 input uncertain parameters, the definition of around 40 correlations (static, statistical) and 11 constraints between input data.

The Monte-Carlo technique used within the benchmarks has appeared to be user-friendly and straightforward to implement. It gives the possibility to consider a spectrum of variation of selected parameters and offers a wide range of graphic output.

Thus, the use of Monte-Carlo technique for both benchmarks has been very beneficial and adequate to get a very good understanding of the behaviour of the global system in terms of propagation of uncertainties using both uncertainty analysis (UA) and sensitivity analysis (SA). For the uncertainty analysis (UA) the following indicators have been used and found useful:

- quantiles, giving the uncertainty and shape of the results (time evolution, peak, time to the peak, ...),
- pdfs and ccdfs, giving the distribution of the results,
- various moments such as kurtosis and coefficient of skewness, characterizing the shape of the distribution (flatness, asymmetry).

And for the sensitivity analysis (SA):

- scatter-plots, giving a first impression of the sensitivity of the output results regarding the input data parameters,
- statistical coefficients such as Pearson, PCC, SRC, Spearman, PRCC, SRRRC, ..., analyzing the linearity or monotony of the output results and identifying the relevant input parameters and their ranking,
- Monte Carlo filtering statistics (Mann-Whitney test and Smirnov test) providing hints about the regions of different input parameters associated to the largest values of the output variables considered,
- Cobweb plots supporting with visual information numeric results obtained via Monte Carlo filtering techniques,
- Contribution to the sample mean plots (CSM plots) identifying input parameters whose different regions contribute unevenly to the output variable means (indicating important first order sensitivity indices),
- Different SA techniques showed a remarkable degree of agreement in the identification of relevant input parameters.

As regards the results obtained in the UA and SA performed by both partners in Benchmark 1 and Benchmark 2, the following conclusions may be drawn:

- for ¹²⁹I in the radial direction, a very good agreement has been found between Benchmark 1 and Benchmark 2 between both codes (Alliances and GoldSim) for the uncertainty analysis (UA) as well as the sensitivity analysis (SA). It can also be generally concluded that the molar rates in the outer layer are controlled by transport characteristics associated with the clay formation. In the axial direction there is an acceptable degree of agreement between Alliances and GoldSim, but for the sensitivity analysis there is a large difference. It must be kept in mind that the JRC analysis relied on input from Andra's 3D analysis to assess the longitudinal flow. The sensitivity analysis reveals that there is no dominant rank indicator which clearly indicates the more complex structure of the disposal cell pathway. Differences are most likely due to the strong simplification done with GoldSim. To model this flow requires in principle a 3D model as was done by Andra.

- for ^{79}Se in the radial direction the agreement for the uncertainty analysis between Alliances and GoldSim is very poor in Benchmark 2 in the innermost layers. This is probably due to the differences in the sorption considered in the concrete. In the outer layers both sets of results are closer, though some differences remain, especially in the highest part of the output variables. The different ways of sampling (not including some correlations in the JRC analysis and the different way of implementing constraints) may explain a significant part of the differences. In both cases, results obtained are higher than in Benchmark 1. Despite the UA differences, the SA results agree reasonably well for outer and inner layers. In the axial direction the disagreement is very large for UA and SA. This is hardly surprising since it includes the reason for the disagreements in the innermost radial layers and the known limitation in the axial flow modelling inherent in GoldSim model.

The two benchmarks have shown that the Monte-Carlo technique is appropriate for “simple cases” and still feasible and applicable for more “complex cases” using 3D numerical tools (more realistic geometry in the case of the second benchmark), despite the large number of simulations required. This is also possible due to the efficiency and constant improvement of computers performance. At the same time, the Monte-Carlo technique has stressed certain limitations of multi-1D codes (compared to “full” 3D codes), especially when an accurate representation of the advective pathway is involved and necessary.

Despite the large number of simulations required for the Monte-Carlo technique, it is currently being applied to problems including more complexity such as unsaturated conditions with gas generation leading to stronger non linearities. In parallel to this technique and in case this would be necessary, the use of alternative or complementary techniques has been tested such as the meta-models based on the response surfaces (neural networks, Chaos polynomials) that allow an efficient way of generating a large number of simulations at a relatively low cost.

8 References

- [1] PAMINA: Performance Assessment Methodologies in Application of to Guide the Development of the Safety Case, EURATOM Integrated project Contract No. FP6-036404, Annex 1 Description of Work.
- [2] Andra, Dossier 2005 Argile – Synthesis report : Evaluation of the feasibility of a geological repository (2005)
- [3] Andra, Dossier 2005 Argile – Safety evaluation of a geological repository (2005)
- [4] Andra, Dossier 2005 Argile – Phenomenological evolution of a geological repository (2005)
- [5] Andra, Dossier 2005 Argile – Architecture and management of a geological repository (2005)
- [6] G. Pepin, F. Plas, S. Prváková and K-F Nilsson, Milestone M 4.3.1 First Benchmark specification for the uncertainty analysis based on the example of the French clay site (April 2007)
- [7] G. Pepin, F. Plas, S. Prváková and K-F Nilsson, Milestone M 4.3.3 Second Benchmark specification for the uncertainty analysis based on the example of the French clay site (May 2008)
- [8] R. Bolado-Lavin, A. Cotescu-Badea, Deliverable D2.1.B.2, Development and testing of a template to present PA results (2009)
- [9] A. Cotescu-Badea, R. Bolado-Lavin, Milestone M2.1.D.4, Review of sensitivity analysis methods and experience (2008)
- [10] R. Bolado, W. Castaing and S. Tarantola, Contribution to the sample mean plot for graphical and numerical sensitivity analysis. *Reliability Engineering & System Safety* 94: 1041-1049 (2009)